



# The classical turbidite outcrop at San Clemente, California revisited

**DOI:**

[10.1016/j.sedgeo.2016.10.001](https://doi.org/10.1016/j.sedgeo.2016.10.001)

**Document Version**

Accepted author manuscript

[Link to publication record in Manchester Research Explorer](#)

**Citation for published version (APA):**

Li, P., Kneller, B. C., Hansen, L., & Kane, I. (2016). The classical turbidite outcrop at San Clemente, California revisited: An example of sandy submarine channels with asymmetric facies architecture. *Sedimentary Geology*. <https://doi.org/10.1016/j.sedgeo.2016.10.001>

**Published in:**

Sedimentary Geology

**Citing this paper**

Please note that where the full-text provided on Manchester Research Explorer is the Author Accepted Manuscript or Proof version this may differ from the final Published version. If citing, it is advised that you check and use the publisher's definitive version.

**General rights**

Copyright and moral rights for the publications made accessible in the Research Explorer are retained by the authors and/or other copyright owners and it is a condition of accessing publications that users recognise and abide by the legal requirements associated with these rights.

**Takedown policy**

If you believe that this document breaches copyright please refer to the University of Manchester's Takedown Procedures [<http://man.ac.uk/04Y6Bo>] or contact [uml.scholarlycommunications@manchester.ac.uk](mailto:uml.scholarlycommunications@manchester.ac.uk) providing relevant details, so we can investigate your claim.



## Accepted Manuscript

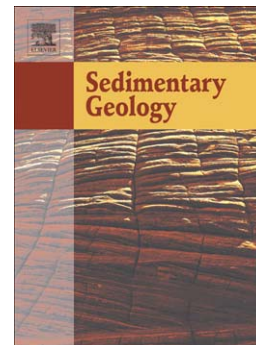
The classical turbidite outcrop at San Clemente, California revisited: An example of sandy submarine channels with asymmetric facies architecture

Pan Li, Benjamin C. Kneller, Larissa Hansen, Ian A. Kane

PII: S0037-0738(16)30079-3  
DOI: doi:[10.1016/j.sedgeo.2016.10.001](https://doi.org/10.1016/j.sedgeo.2016.10.001)  
Reference: SEDGEO 5120

To appear in: *Sedimentary Geology*

Received date: 23 May 2016  
Revised date: 4 October 2016  
Accepted date: 5 October 2016



Please cite this article as: Li, Pan, Kneller, Benjamin C., Hansen, Larissa, Kane, Ian A., The classical turbidite outcrop at San Clemente, California revisited: An example of sandy submarine channels with asymmetric facies architecture, *Sedimentary Geology* (2016), doi:[10.1016/j.sedgeo.2016.10.001](https://doi.org/10.1016/j.sedgeo.2016.10.001)

This is a PDF file of an unedited manuscript that has been accepted for publication. As a service to our customers we are providing this early version of the manuscript. The manuscript will undergo copyediting, typesetting, and review of the resulting proof before it is published in its final form. Please note that during the production process errors may be discovered which could affect the content, and all legal disclaimers that apply to the journal pertain.

# The classical turbidite outcrop at San Clemente, California revisited: an example of sandy submarine channels with asymmetric facies architecture

Pan Li <sup>a,\*</sup>, Benjamin C. Kneller <sup>a</sup>, Larissa Hansen <sup>a</sup>, Ian A. Kane <sup>b</sup>

<sup>a</sup> *Department of Geology and Petroleum Geology, University of Aberdeen, AB24 3UE, UK*

<sup>b</sup> *School of Earth, Atmospheric and Environmental Sciences, University of Manchester, M13 9PL, UK*

## Abstract

A 1.1-1.2 km long, 3-15 m thick exposure of the late Miocene to Pliocene Capistrano Formation crops out at San Clemente, California, providing a superb example of submarine channel elements with an asymmetric cross-sectional facies distribution. Coarser-grained, thicker bedded and more amalgamated channel axial deposits are partitioned towards one side of channel elements (200-400 m wide), whilst finer-grained and thinner bedded channel margin deposits are partitioned towards the other side. Two end-member types of silty channel-base and intra-channel drapes are recognized, namely, bypass drapes and deposition drapes. There are both draping silty turbidites that show either strong (bypass drapes) or insignificant (deposition drapes) evidence of erosion and/or sediment bypass during deposition. Bypass drapes and deposition drapes are interpreted to result from flow bypass and flow stratification, respectively, and have significantly different implications for reservoir connectivity and down-dip sediment transport. Channel elements are nested to form two channel complexes. Channel complex 1 comprises four channel elements and shows a vertical aggradation dominated stacking pattern, whilst channel complex 2 comprises five channel elements and shows a mixed lateral migration/vertical aggradation stacking pattern. This study also suggests that these exposures represent only a fragment of a larger channel complex set that might bear varying degrees of resemblance to its formative geomorphic channel(s) on the paleo-seafloor. The reinterpretation of this classic outcrop provides valuable insight into other turbidite channel systems at outcrop and in the subsurface, both in a sedimentological and applied context.

**Keywords:** Turbidite; Slope channels; Terrace; Facies architecture asymmetry; Coarsening/thickening upward trends, San Clemente; Deep-water outcrop

## 1. Introduction

Submarine channels are long-lived conduits for the transport of clastic sediments and organic material from fluvial and shallow marine environments to the deeper parts of basins. Their role in the transport of sediment, organic carbon and, increasingly, pollutants is important to understand. In addition, channels focus flows that pose a hazard to seafloor infrastructure, and their deposits may constitute important hydrocarbon reservoirs. Studies of modern and subsurface deep-water systems have provided significant insights into turbidite channels in terms of their morphologies, initiation, large- and small-scale stratigraphic architecture and evolution (e.g., Abreu et al., 2003; Deptuck et al., 2003, 2007; Babonneau et al., 2004; Cross et al., 2009; Mayall et al., 2010; Paull et al., 2011, 2013; Kolla et al., 2012; Maier et al., 2012; Gamberi et al., 2013; Janocko et al., 2013). However, bed-scale cross-sectional variability, such as changes in facies architecture from channel axis to channel margin, and their causal depositional processes, are in general poorly-constrained by these datasets due to limitations of scale or data resolution. In these respects, well-exposed outcrops can provide more detailed insights (e.g., Hickson and Lowe, 2002; Gardner et al., 2003; Grecula et al., 2003; Arnott, 2007; Kane et al., 2009; Jobe et al., 2010; Pyles et al., 2010; Hodgson et al., 2011; Hubbard et al., 2014). Nonetheless, to our knowledge, outcrop studies on submarine channels (especially sandy submarine channels) with asymmetric facies architecture and well-developed intra-channel tabular deposits are rarely reported and investigated in detail (Walker, 1975; Hein and Walker, 1982; Sullivan et al., 2000; Pyles et al., 2010; McHargue et al., 2011; Hodgson et al., 2011; Fildani et al., 2013). In this study, we document such channels in outcrops of the late Miocene-Pliocene Capistrano Formation exposed at San Clemente, California, USA. Specifically, we document channel fill geometries, sedimentary facies and facies distributions, bed to bedset scale correlations, with the aim of answering the following specific questions: (1) How does submarine channel architecture vary from the channel axis to the channel margin at channel element scale? (2) What are the associated depositional processes for emplacing various types of drapes? (3) What are the stacking patterns of those channel elements? (4) Do the channel-fills at outcrop represent most of the system or just a small slice thereof? If it is the latter, then what are the likely cross-sectional dimensions of the entire depositional system? And (5) what are the new implications of this reinterpretation of the classical outcrop for hydrocarbon exploration and production?

## 2. Geological setting

### 2.1. Regional setting

During deposition of the late Miocene-Pliocene Capistrano Formation (~10-4 Myr), the study area in San Clemente lay within a N-S trending marine embayment (the Capistrano Embayment) (Fig. 1a). The embayment is characterized by a physiographic and structural trough bounded by the San Joaquin Hills to the west and the Cristianitos Fault to the east (Ingle, 1971; Ehlig, 1979; Bouroullec and Pyles, 2010). Along the present day coastline, the embayment extends from Dana Point eastward to the Cristianitos Fault (c. 15 km wide) and narrows northwards until it terminates at the Santa Ana Mountains. The embayment extends southward from the coastline and merges with a deeper open ocean basin offshore (Ehlig, 1979).

Prior to deposition of the Capistrano Formation, the area subsequently occupied by the Capistrano Embayment was part of a larger closed basin below sea level that was characterized by laminated and diatomaceous mudstone of the Monterey Formation, which was deposited under oxygen-deficient conditions at middle to lower bathyal water depths (Ingle, 1971; Ehlig, 1979) (Fig. 2). During the late Miocene, the Capistrano Embayment, with a submarine scarp on its eastern side, began to develop as a result of movement along the Cristianitos Fault. The sediments of the Capistrano Formation were subsequently deposited in the Capistrano Embayment until the early Pliocene when movement on the Cristianitos Fault ceased. During this period, sediment gravity flows transported sediment westward down the submarine scarp along the Cristianitos Fault. These flows formed muddy slope deposits and coarser-grained slope channel-fills on the east side of the embayment, part of which crops out in the study area (Ehlig, 1979; Malone and Alba, 1979; Camacho et al., 2002; Campion et al., 2005). Foraminiferal assemblages and radiolarian tests from the Capistrano Formation around Dana Point indicate middle or lower bathyal paleo-water depths of approximately 900 m to 2000 m during deposition (White, 1956, 1971; Ingle, 1971). The prevailing deep-water conditions were followed by at least 1000 m of uplift during the Pliocene to Pleistocene, resulting in widespread erosion and development of the unconformable contact of the Capistrano Formation with the overlying Pleistocene marine terrace deposits (Campion et al., 2005).

## 2.2. Study Area

The Capistrano Formation is well exposed on the 1.1-1.2 km long and 3-15 m high, NNW-SSE to NW-SE orientated sea cliffs at San Clemente State Beach in the city of San Clemente, California, USA (Fig. 1b). It consists of three primary sections, corresponding to sections A, B, and C in this study, which are dissected by three gullies and a parking lot that provide a partial 3D view of the outcrop (Fig. 1b). These sections show that the exhumed Capistrano Formation in the study area is largely a sand-dominated turbidite channel system that features a wide range of channel fills, ranging in grain size from strongly bioturbated mudstone to boulder-sized conglomerates (Walker, 1975; Busby et al., 1998; Camacho et al., 2002; Campion et al., 2005, 2007) (Figs. 3, 4; Table 1). Bedding dips within channel fills and the enclosing Monterey Formation mudstones are largely sub-horizontal except close to the channel edges, where beds within the channel fills may dip away from the channel edges towards channel axes at up to 15° to 20°. The channel fills are overlain at the top of the cliffs by sandy or gravely deposits of Pleistocene marine terrace origin (Walker, 1975) (Fig. 2). A 300-400 m gap separates section C from the outcrops to the northwest. These outcrops were first described by Camacho et al. (2002) and recently by Jester (2013), but are not included in this study due to the uncertainty in correlation across the exposure gap.

Numerous studies have been undertaken on the well-exposed channel fills within sections A, B and C since 1971 (Weser, 1971; Walker, 1975; Hess, 1979; Clark and Pickering, 1996; Busby et al., 1998; Campion et al., 2000, 2005, 2007; Camacho et al., 2002; Posamentier and Walker, 2006; Bouroulllec et al. 2007; Chapin and Keller, 2007; Stewart et al., 2008; Jester, 2013; Pickering and Hiscott, 2016). An overall marine slope setting for the channel fills has been envisaged in the publications since 1998, and is accepted here. However, there are markedly contrasting views concerning architecture, sedimentary processes, and geometry of the channel fills. We revisit the previously interpreted outcrop (sections A, B, and C) in the hope of shedding new light on these issues based on our field data and recent advances in the understanding of submarine channels.

## 3. Data and Methodology

Three photomosaics of beach-facing cliffs and several complementary ones from the cross-cutting gullies were used for bed correlation and facies architecture analysis. Twenty-eight sections totaling 215 m were measured in the field at a scale of 1:10 with some selected intervals logged at 1:5 for more detailed sedimentological analysis. Inaccessible sections were documented as “photo logs”,

which entailed taking high-resolution photos with measured scales in order to constrain the thickness and distributions of the main facies. Bed- to bedset-scale correlation and thickness analysis was undertaken for the continuously exposed part of the outcrop by walking out beds in the field, visual inspection of logged sections, and surface tracing using high-resolution photomosaics and/or digital mapping. In digital mapping, a laser rangefinder was integrated with a handheld pocket PC with an embedded global navigation satellite system (GNSS) receiver, enabling positions to be captured with 1 cm-100 cm accuracy in x, y, and z directions. Where possible, the orientation of channel edges was measured on their excavated parts and/or via digital mapping along 3D exposures. A total of twenty-eight paleoflow directions were measured based on 3D ripple cross lamination, cross bedding, clast imbrication and soft-sediment deformation such as slump folds and flame structures.

#### 4. Hierarchy and Terminology

An architectural hierarchy of four scales is applied to the turbidite channel system at San Clemente, based on the hierarchical schemes proposed by Campion et al. (2000, 2005), and Sprague et al. (2002, 2005) (Fig. 3). Increasing in scale, it consists of facies, channel elements, channel complexes and channel complex sets (Fig. 3). Facies comprise a bed or packages of bed that share similar sedimentary features. They generally form the basic mappable packages at San Clemente. Channel elements comprise individual channel fills, representing the fill of long-lived conduits for sediment transport (Mutti and Normark, 1987; Macauley and Hubbard, 2013). Channel elements are characterized by distinct sub-environments, including channel axis and channel margin that commonly show different facies distributions (Fig. 3). Channel elements with similar affinity (architecture and dimensions) are nested to form a channel complex that is usually characterized by distinct channel element stacking patterns. Two or more nested channel complexes within a particular stratigraphic interval comprise a channel complex set (Campion et al., 2000, 2005; Sprague et al., 2002, 2005; Abreu et al., 2003). The outcrop in this study forms one channel complex set that comprises two channel complexes, which each consist of four and five channel elements (Fig. 3).

#### 5. Facies: results and interpretations

Based on the measured sections and photomosaics, six main facies have been recognized within the turbidite channel fills: (F1) bedded siltstone; (F2) silt-rich thin-bedded deposits; (F3) sand-rich thin-bedded deposits; (F4) medium- to thick-bedded sandstone; (F5) conglomerate; and (F6) mudstone-clast-rich facies, including mudstone-clast-rich conglomerate (F6-a) and mudstone-clast-rich

sandstone (F6-b). Their bed-scale characteristics (Fig. 4) and process-based interpretations are summarized in Table 1. Fine-grained facies F1 and F2 are characterized by strong bioturbation, normal grading, and lamination, and are attributed to low-density turbidity currents (cf., Bouma, 1962). F4 features coarse-tail grading/no grading, massive structures with common soft sediment deformation structures and no or minor bioturbation, suggesting rapid deposition from high-density turbidity currents (cf., Lowe, 1982; Mutti, 1992; Kneller and Branney, 1995; Talling et al., 2012). F3 shows characteristics intermediate between F1/F2 and F4 in terms of grain size, sedimentary structures and bioturbation (Fig. 4; Table 1.), suggesting deposition from low- to high- density turbidity currents. F5 is characterized by coarse grain size (up to boulder), common erosive bases with ripped up mudstone clasts, and is attributed to bypassing turbidity currents (cf., Mutti and Normark, 1987; Stevenson et al., 2015). F6-a is attributed to channel margin slump or freezing of mud-clast-laden turbidity currents (cf., Walker, 1975; Camacho et al., 2002; Campion et al., 2005; Chapin and Keller, 2007), considering its sandy matrix, sub-angular to angular ripped up mudstone clasts, overlying and underlying turbiditic beds and the context of slope channel setting. F6-b is interpreted to record bypassing turbidity currents based on its common intercalation with coarse-grained laminated sandstone (cf., Mutti and Normark, 1987; Stevenson et al., 2015).

## **6. Channel elements**

### **6.1. Description**

In the study area, channel elements are recognized by pronounced erosional surfaces with relief typically up to 5-8 m that are draped or onlapped by multiple event beds, particularly strongly bioturbated bedded siltstone packages up to 2.5 m thick. We first describe the general characteristics of all the channel elements in terms of their geometry and facies distributions and then document the bedding patterns from the most completely preserved element (channel element 9). This element is used as a primary example for interpretation of facies architecture and sedimentary processes.

#### **6.1.1 Characteristics of channel elements**

Apart from channel element 9, only the southern channel edge of each channel element is exposed. Those channel edges generally can be traced for 40 m to 120 m along strata before dipping into the subsurface to the north (Fig. 5), and show an apparent progressive shift towards the north based on their geometries. The southern edge of channel element 1 is steeper than the others and is incised into the Monterey Formation, while the rest cut into previous channel elements, resulting in the



presence of some elevated flat erosional surfaces which are overlain by largely flat-lying deposits (Channel elements 2 and 6 in Fig. 5). For channel element 9, both its northern and southern edges crop out, giving an apparent width of approximately 510 m and a minimum thickness of ca. 15 m. Additionally, the southern edge appears to show slightly gentler inclination ( $1^{\circ}$  to  $5^{\circ}$  especially at its upper part, see Fig. 5) than the northern edge ( $5^{\circ}$  to  $15^{\circ}$ ), yielding the appearance of a slightly asymmetric cross-sectional profile.

Facies within channel elements have been mapped on the three primary photomosaics (sections A, B, and C in Fig. 5). Channel element 1 is dominated by thin-bedded heterolithic deposits (F2 and F3) with subordinate medium-bedded massive sandstone (F4) and mudstone-clast-rich sandstone (F6-b); it is characterized by a number of intra-channel erosional surfaces with relief of tens of centimetres. Beds have a dip of a few degrees towards the north and lap abruptly against the channel edge towards the south. Channel elements 2, 5 and 6 consist mainly of facies F2 and F3, F1 and F4 (Fig. 5). The amalgamated sandy facies (F4) are mainly present in the lows confined by erosional surfaces, whereas the non-amalgamated muddier and thinner bedded facies (F1, F2, F3) overlie the elevated flat surfaces, with only siltstone (F1) draping the relatively steep channel edges. In contrast, channel elements 3, 4, 7 and 8 comprise much coarser and thicker bedded facies, including medium- to thick-bedded sandstone (F4) and conglomerate (F5). Amalgamation and/or erosional surfaces are common, some of which are draped by laminated siltstone (F1) or mudstone-clast rich conglomerate (F6-a) (Fig. 5). In channel element 9, both coarser, more amalgamated facies and finer, less amalgamated facies are present and are discussed in detail below.

### **6.1.2 Bedding patterns in channel element 9**

From the southern end of the parking lot to the southern edge of channel element 9 (right side of Fig. 6), six bed packages are recognized and correlated (Figs. 6, 7). Sandstone dominated package 1, comprised mainly of facies F4 with common mudstone rip-up clasts, is partially exposed. It is locally truncated by a continuous intra-channel surface that appears to be draped by thin-bedded package 2 (F1, F2, F3) (Fig. 6). Package 2 and individual beds within it do not show a systematic trend in lateral thickness variations (Fig. 8). In contrast, the overlying package 3 is made up of amalgamated sandstone (F4) and displays an overall wedge-shaped geometry, although beds are more tabular in proximity to channel element 9's southern edge, towards which thicknesses of bed packages 2-5 tend to converge (Figs. 6, 8). Notably, bed packages 4, 5, and 6 show tabular geometries without clear

undulating scours and extend across the entire correlation panel in Fig. 6. Also notable is that packages 2 to 5 converge and transition into strongly bioturbated silty facies towards the southern edge of channel element 9 (Figs. 6, 7).

Overall, the finer-grained less amalgamated margin of CE 9 consists of two components. The lower, (bed packages 1, 2 and the lower part of 3), includes a set of depositional surfaces with a corrected dip of 3° to 4° towards the axis (see Fig. 6). This package has accreted away from the gently dipping southern edge of this channel element. This set of inclined surfaces is overlain by flat-lying tabular deposits of packages 4, 5 and 6.

From the northern end of the parking lot to the northern edge of channel element 9 (left side of Fig. 6), a different bedding pattern is present: lenticular, medium- to thick-bedded, medium- to coarse-grained sandstone and conglomerate with widespread ripped up mudstone clasts (F4, F5), as observed by previous workers (Walker, 1975; Campion et al., 2000; Camacho et al., 2002, amongst others) (Figs. 6, 7). They are ungraded or coarse-tail graded with erosive bases and thin laminated tops preserved locally. Where present, fine-grained thin-bedded heterolithic deposits (F2, F3) are truncated and form discontinuous lenticular bodies (Figs. 5, 6). No continuous tabular beds are present in the successions here.

The patchy outcrops around the approximately 120 m long parking lot allow us to tentatively link the sections on either side (Fig. 6). Despite a degree of uncertainty concerning correlation between them, these two sections illustrate the lateral variations in internal architecture of channel element 9.

## **6.2. Interpretation**

### **6.2.1 Architecture of channel elements**

Using channel element 9 as a representative channel element with consideration of the characteristics of other elements, a channel-element scale architectural model with asymmetric facies distributions is proposed (Fig. 9). It consists of two distinct channel sub-environments, including the coarser-grained and more amalgamated channel axis and the finer-grained and less amalgamated channel margin. Their distributions collectively record an asymmetric architectural style with the channel axis located closer to the more steeply dipping channel edge, while the channel margin composes the rest of the channel element (Figs. 6, 9). This is comparable to some other well-documented channel-fills where varying degrees of facies architecture asymmetry exist (e.g.,

Babonneau et al., 2010; Jobe et al., 2010; Pyles et al., 2010; McHargue et al., 2011; Paull et al., 2013; Reimchen et al., 2016).

Similarly to channel element 9, channel element 1 (the exposed part of which represents only the finer-grained margin) comprises packages showing dips of  $3^{\circ}$  to  $5^{\circ}$  towards the inferred axis (see Fig. 5c). This bears very close comparison with structures reported from the Congo channel by Babonneau et al. (2010), where low angle (ca.  $3^{\circ}$ ) reflectors dip towards the channel axis and are overlain by flat-lying terrace deposits. The Congo channel also shows comparable asymmetry to that which we invoke here.

Channel element dimensions can only be inferred, due to the incomplete exposure and the need to correct their apparent widths (i.e., 550 m). Considering an outcrop orientation of  $340^{\circ}$ , average paleoflow of  $318.5^{\circ}$  and average channel edge of  $284^{\circ}$  (Table 3), the true width of channel element 9 is calculated to be around 200 to 400 m. In addition, the projection of both edges of channel element 9 into the subsurface to form a smooth arc yields a few meters buried depth. Together with the exposed channel depth ( $\sim 15$  m), it suggests an estimate of around 20 m for the minimum channel depth without taking into account the potentially eroded parts above the outcrop. This is similar to the estimate (20-25 m) provided by Walker (1975) for the same channel element. Despite the uncertainties, both the estimated channel width and depth fall within the ranges compiled from outcrop and seismic data by McHargue et al. (2011).

### **6.2.2 Sedimentary processes in channel elements**

At the channel axis, very coarse grain sizes, including coarse-grained sandstone, pebbly sandstone and conglomerate, indicate deposition from fast-moving, thalweg-confined gravelly and sandy flows (Walker, 1975; Camacho et al., 2002; Campion et al., 2005); common structureless, ungraded or coarse-tail graded thick beds suggest deposition from waning or quasi-steady, high-concentration turbidity currents with high sediment fallout rates (cf., Lowe, 1982; Mutti, 1992; Kneller and Branney, 1995; Talling et al., 2012). Additionally, abundant mudstone rip-up clasts, basal pebble lags, and amalgamation/erosion surfaces with or without silty drapes are suggestive of flow bypass and/or erosion (cf., Mutti and Normark, 1987; Beaubouef et al., 1999; Camacho et al., 2002; Campion et al., 2005; Stevenson et al., 2015). Large volumes of finer-grained sandy and muddy sediment are thought to have been bypassed by the channels, as in channels showing similar characteristics elsewhere (e.g., Mutti and Normark, 1987; Hodgson et al., 2011; Hubbard et al., 2014; Stevenson et al., 2015).

At the channel margin, massive, coarse-tail graded medium- to thick-bedded sandstones with common soft sediment deformation structures, but lacking evidence for significant erosion, indicate high fall-out rates of sand from high-concentration turbidity currents (cf., Lowe, 1982) (Fig. 6). Intercalated thin-bedded turbidites draping intra-channel erosion surfaces represent deposition from muddy tails of bypassing turbidity currents and/or the lateral low-concentration fine-grained equivalents of sandier turbidity currents in the thalweg (cf., Mutti and Normark, 1987; Beaubouef et al., 1999; Barton et al., 2010; Hubbard et al., 2014; Stevenson et al., 2015) (Fig. 6). The strongly bioturbated silty drapes at channel edges are suggestive of slow deposition from upper dilute portions of turbidity currents (cf., Walker, 1975; Campion et al., 2000, 2005; Camacho et al., 2002; Grecula et al., 2003; Callow et al., 2014; Stevenson et al., 2014, 2015). Marginal tabular deposits are attributed to deposition on elevated flat intra-channel surfaces by lateral lower-energy equivalents of flows at the channel thalweg, and are thus interpreted as terrace deposits (cf., Walker, 1966, 1975; Babonneau et al., 2002, 2004, 2010; Paull et al., 2013; Hubbard et al., 2014; Hansen et al., 2015) (Figs. 5, 6). Alternatively, the tabular sediments might represent erosional remnants of passive channel backfills, as proposed by Clark and Pickering (1996) for the sheet sand within the Eocene Ainsa channels in Spain.

### **6.2.3 Origins and recognition criteria of drapes in channel elements**

The origins of the prominent drapes in the study area have been debated in previous studies (cf., Walker, 1975; Campion et al., 2000, 2005; Camacho et al., 2002; Jester, 2013). In this study, we recognized two end-member drape types, “bypass drapes” (sensu Barton et al., 2010) and “deposition drapes” (cf., “convergent drapes” of Barton et al., 2010; drapes from “underfit” flows of Hubbard et al., 2014), which have different character, formation mechanisms and recognition criteria.

Bypass drapes, comprised mainly of siltstone with subordinate very fine- to medium-grained sandstone, tend to include features indicating erosion or bypass, such as rip-up clasts of mudstone or sandstone, multiple erosional surfaces and coarse-grained facies, or are interstratified with deposits showing such characteristics (Fig. 10). They drape channel bases (such as the drapes overlying channel element 4), or intra-channel erosional surfaces (e.g., Fig. 10, basal siltstone of package 2 in Fig. 6). Bypass drapes are interpreted to form when the head and body of the flow have mainly bypassed and the tail of flow deposits silty sediment (cf., Mutti and Normark, 1987; Campion et al., 2005; Barton et al., 2010; Hubbard et al., 2014; Stevenson et al., 2014, 2015) (Fig. 11a). In this

scenario, the drape does not laterally grade into coarser and thicker bedded sands towards the channel axis; rather, it extends without much change in grain size from the axis towards the margin up to the highest point that the flow reached. Bypass drapes can occur either during the initiation or at the filling stage of channel development, but are commonly better developed prior to the main filling stage (cf., Campion et al., 2005; Barton et al., 2010; Hubbard et al., 2014; Stevenson et al., 2014, 2015).

In contrast to bypass drapes, deposition drapes, the dominant type of drapes in the study area, are found not to be related to multiple erosion or bypass indicators mentioned above. Deposition drapes comprise mainly siltstone with subordinate very fine-grained sandstone, and show distinct convergent geometry towards the channel edge with bed dips commonly decreasing upwards (cf., Beaubouef et al., 1999; Campion et al., 2005; Barton et al., 2010; Alpak et al., 2013; Stevenson et al., 2015) (Fig. 7d). In addition, some beds within deposition drapes can be confidently traced into sandstone or thin-bedded heterolithic deposits towards the channel axis (Fig. 7e, f), suggesting the coeval sedimentation of the deposition drapes with the sands towards the channel axis (Walker, 1975; Camacho et al., 2002). In this scenario, the head, body and tail of the flow deposit coarser sandy sediment towards the channel axis and finer silty sediment from the upper part of the flow towards the channel margin, contemporaneously (Camacho et al., 2002; Stevenson et al., 2014) (Fig. 11b). This type of drape is expected to occur mainly during the filling stage of channel elements, when flows are more depositional (cf., Barton et al., 2010; Alpak et al., 2013; Hubbard et al., 2014).

Based on the above discussion, criteria for distinguishing deposition and bypass drapes at outcrop could be established based mainly on their different grain size range, lateral geometries (grading laterally into axial sands or not), distributions (in the channel axis or margin), with or without associated erosion/bypass features, and upward trends of bed dips, and are summarized in Table 2.

#### ***6.2.4 Origins of coarsening/thickening upward successions in channel elements***

A number of studies have reported coarsening and/or thickening upward successions in the margins of submarine channels (e.g., Pickering, 1982, 1986; Beaubouef et al., 1999; Sullivan et al., 2000; Grech et al., 2003; Campion et al., 2005; Pyles et al., 2010; McHargue et al., 2011; Hubbard et al., 2014; Bain and Hubbard et al., 2016). Similar vertical trends are observed in the channel margins of channel elements 2 and 9 (Figs 5c, 5d, 6, 10a, 10b), as also recognized by Walker (1975) and Campion et al. (2005). They interpreted those vertical successions in the study area as a result of

lobe progradation and channel backfilling, respectively. Here, we propose two alternative formative mechanisms.

One possible mechanism for the coarsening and/or thickening upward successions in the study area is lateral expansion of intra-channel locus of coarser and sandier deposition towards the channel margin (cf., Pickering, 1982, 1986; Elliot, 2000; Sullivan et al., 2000; Lien et al, 2003; Hubbard et al., 2014). It could occur as a result of the decreasing channel margin relief through the evolution of a channel (cf., Pickering, 1982, 1986; Sullivan et al., 2010; Hubbard et al., 2014). As such, sandier and denser suspensions concentrated in the lower part of stratified turbidity currents can more often make their way to the adjacent higher channel margin as the relief between them decreases. This could produce thickening and/or coarsening-upward successions at the channel margin, and is likely to happen at the later filling stage of channel element evolution as the axial part of the channel aggrades more quickly than the margin (cf., Pickering, 1982, 1986; Hubbard et al., 2014) (Fig. 6).

Another possible mechanism is increasing flow magnitude due to extrabasinal or intrabasinal controls (e.g., sea level, climate, seafloor gradient, magnitude of mass wasting) (cf., Pickering, 1986; Kane et al., 2007; Pyles et al., 2010). Thicker flows could permit their sandy suspensions to extend to the margin, forming sandier and thicker beds that overlie the thinner and muddier sediments (e.g., depositional drapes) emplaced by earlier smaller flows, yielding coarsening and/or thickening successions at the channel margin (Fig. 6). This is expected to be more likely to occur at the earlier filling stage of channel element evolution when waxing flows tend to be more common (cf., Pickering, 1986; Grecula et al., 2003; Campion et al., 2005; Pyles et al., 2010).

## **7. Channel complexes**

Channel elements are stacked to form channel complexes. Interpretation of the stacking patterns of channel elements, however, is equivocal or misleading based solely on incomplete exposures like the outcrop examined in this study, as schematically illustrated in Fig. 12. This is evidenced by the contrasting stacking patterns proposed in the study area (cf., Walker, 1975; Campion et al., 2000, 2005; Camacho et al., 2002; Jester, 2013). Here, we approach this problem by considering both the exposed and inferred missing counterparts of these channels. This is achieved based on the assumption that coarser-grained, more amalgamated deposits tend to occur lower and closer to the channel axis, whilst finer-grained, less amalgamated deposits tend to be higher and closer to the channel margin (Fig. 9), as argued by many other workers in the study area (e.g., Walker, 1975;

Campion et al., 2000, 2005; Camacho et al., 2002). This assumption is supported by the most complete channel fills (channel element 9) in the study area, and numerous examples elsewhere (e.g., Mutti and Normark, 1987; Pyles et al., 2010; Hodgson et al., 2011; Paull et al., 2013; Hubbard et al., 2014).

Based on the mapped facies distributions (Fig. 5) and the general supposition outlined above, we interpret exposures of channel elements 1 and 2 to include only slices through the margins, with their axes buried below the outcrop. Similarly, exposures of channel elements 3 and 4 include only slices through the axes, with their margins eroded from above the outcrop. Taken together, channel elements 1 to 4 display an aggradational stacking pattern, although the system shows a certain degree of lateral migration from channel element 1 to channel element 2 (Fig. 13). Applying the same principle to the rest of the exposure suggests that channel elements 5 to 9 are characterized by a combination of both lateral migration and vertical aggradation (Fig. 13). If the channel system had migrated only laterally, as suggested by other researchers (Walker, 1975; Clark and Pickering, 1996; Campion et al., 2000, 2005, 2007), the outcrop would slice through the same stratigraphy for each channel element, and each would therefore display similar facies distribution patterns in outcrop; this is inconsistent with what is observed (see Fig. 5). Based on the above inferred stacking patterns of channel elements and consideration of paleoflow directions and channel edge orientations (Table 2), channel elements 1 to 4 are interpreted to form one channel complex (channel complex 1), characterized by a vertical aggradational stacking pattern. Channel elements 5 to 9 are attributed to another channel complex (channel complex 2) that shows a mixed lateral/vertical migration pattern. Noticeably, channel element 9 shows different orientation from channel elements 5-8 (Table 2). However, it still appears to be nested within channel complex 2 if we project its southern edge above the outcrop, as noted by Walker (1975). The difference in paleoflow indicators is probably a result of either curvature of channel element 9 or different position of channel bends compared to older elements within the same complex, a feature that is very common in the evolution of channel elements (e.g., Stelting et al., 1985; Deptuck et al., 2003, 2007; Janocko et al., 2013).

## **8. Channel complex set**

The two channel complexes form a channel complex set whose southern edge is partially exposed and incises into the bioturbated low-gradient slope mudstone of the Monterey Formation. Its northern edge is presently covered by vegetation, but was reported by Weser (1971) to crop out at around 150-

250 m to the NW of the northern terminus of section C of this study, where it featured a well-defined erosional surface cutting into horizontally bedded siltstone and mudstone and onlapped by massive sandstone and conglomerate (see Fig. A of plate XI in Weser, 1971). It is not clear whether the siltstone and mudstone are slope background deposits of the Monterey Formation or overbank deposits of submarine channels of the Capistrano Formation. In any case, the apparent width of the channel complex set is around 1.1-1.2 km in outcrop. Based on mean outcrop orientation ( $340^\circ$ ) and mean paleoflow direction ( $300^\circ$ ), simple trigonometry (i.e.,  $\text{true width} = \text{apparent width} \cdot \sin(\text{outcrop orientation} - \text{channel orientation})$ ) yields an estimate of around 750 m for the true width of the channel complex set under consideration.

The minimum thickness of the channel complex set could be roughly constrained by projecting its bounding edges into the subsurface to form a smooth circular arc (Camacho et al., 2002) (see Fig. 13). This yields a minimum of 50-60 m thick for the channel complex set examined. It is a rather conservative estimate compared to those of Weser (1971) and Camacho et al. (2002), but the same conclusion can be drawn that the outcrop of turbidite channels of the Capistrano Formation at San Clemente most likely represents a limited portion of a much larger system due to partial burial and outcrop erosion. That said, considering the limitation of outcrop exposure, we prefer to be cautious in interpreting the inferred large channel system preserved in the rock record in terms of the formative geomorphic features (i.e., channels) on the paleo-seafloor (cf., Deptuck et al., 2003; Strong and Paola, 2008; Sylvester et al., 2011; Bain and Hubbard, 2016; Hodgson et al., 2016; and references therein). We suggest that the inferred large channel system in the study area could potentially be established through: (1) a rapidly and/or progressively formed deeply incised channel/canyon with later filling and modification of the confining surface, or (2) a combination of seafloor degradation and aggradation through the protracted evolution of lower-relief submarine channels (Bain and Hubbard, 2016; Hodgson et al., 2016) (cf., Weser, 1971; Walker, 1975; Clark and Pickering, 1996; Campion et al., 2000, 2005; Camacho et al., 2002; Posamentier and Walker, 2006; Jester, 2013; Pickering and Hiscott, 2016).

## 9. Discussion

We have demonstrated cross-sectional features regarding the channel fills in the study area, including asymmetrical facies architecture, different types of drapes, and stacking patterns. Below, we discuss whether and how the two-dimensional stratigraphic architectural features or elements can be



linked to or used to constrain planform sinuosity and one-dimensional vertical profiles, or vice versa. More importantly, we examine the applications of such a holistic approach in the subsurface for development and production within oil and gas fields.

### **9.1. Cross-sectional architecture vs. planform sinuosity**

Several lines of evidence regarding cross-sectional architectural geometry can help constrain the interpretation of channel sinuosity in the study area. Firstly, the photomosaics and measured sections document cross-sectional facies asymmetry in channel element 9 (Figs. 5, 6, 9), and probably the other channel elements also. This facies asymmetry bears strong similarity to that documented in other outcrops (Jobe et al., 2010; Pyles et al., 2010; Alpak et al., 2013), in seismic data (Stelting et al., 1985; De Ruig and Hubbard, 2006) and reproduced experimentally (Straub et al., 2008), where coarser facies are located closer to steeper outer banks of sinuous channels and finer facies are located closer to their gentler inner banks. We therefore propose a degree of channel sinuosity for the turbidite slope channels at San Clemente (cf., Campion et al., 2005; Bouroullec et al., 2007; Jester, 2013). This argument is further supported by the potential terrace deposits (tabular deposits in Fig. 5c-e) observed towards the southern edges (inferred inner bends) of the channel elements. Their common occurrence at inner bends is well-documented in many studies of subsurface systems imaged with seismic data (e.g., Deptuck et al., 2003, 2007) and in modern systems (Babonneau et al., 2004, 2010; Paull et al., 2011, 2013; Maier et al., 2012). The development of deposition drapes on the inferred inner bends lends additional credence to the interpretation of channel sinuosity (cf., Alpak et al., 2013) (Fig. 5). Furthermore, the oblique orientations of channel edges to paleoflow directions (a difference of 14° to 35°) for channel elements 1, 2, 9 are also likely to result from channel sinuosity at meander bends, as those well documented in the Brushy Canyon Formation (Pyles et al. 2010), rather than a result of apparent dip and strike measurements of channel edges (cf., Camacho et al., 2002) (Table 2). However, the modest channel form asymmetry in cross-sectional direction observed in channel element 9 is interpreted to most likely reflect its relatively low sinuosity, based on the correlation between cross-sectional asymmetry and sinuosity that has been empirically established (e.g., Peakall et al., 2000; Abreu et al., 2003; Jobe et al., 2010; Pyles et al., 2010; McHargue et al., 2011) and quantified recently from bathymetric data (Reimchen et al., 2016). The low sinuosity of channel element 9 inferred from the above evidence contrasts with a high sinuosity of 1.7 estimated

by Campion et al. (2005), although a degree of uncertainty concerning the sinuosity of the other channel elements in the study area exists due to limitations of exposure.

## 9.2. Channel stacking patterns vs. vertical successions

The two different patterns of channel stacking recognized here (a vertical aggradation dominated stacking of channel elements 1-4 and a mixed lateral migration/vertical aggradation stacking of channel elements 5-9) are used to explore the effect of variable preservation of channel fills on vertical successions.

For channel elements 5-9, its unidirectional lateral migration with vertical aggradation (channel elements 5-8) reflects lateral shift in loci of deposition of successively younger channels away from those of the older channels towards the cut bank (e.g., of channel element 6 relative to channel element 5 in Fig. 13). As such, the fine-grained marginal parts of younger channels tend to overlie the coarser-grained more axial parts of the older channels, and thus form fining upward successions for composite channel fills of a channel complex (see channel element 5 and channel element 6 in Figs. 5d, 13). The development of channel element 9 complicates the vertical profiles by removing the otherwise fine-grained margins of channel elements 7 and 8. Such fining upward successions are unlikely to be well-preserved or present closer to the cut bank where the coarse-grained channel axis deposits are highly amalgamated (Fig. 13).

For channel elements 1-4, vertical aggradation of channel elements result in cannibalized channel axes and stacked better-preserved channel margins (Fig. 13). In this case, largely similar vertical patterns from the four channel margins are stacked vertically. As a result, no fining or coarsening upward successions for the composite margin of channel complex 1 are present. This contrasts starkly with the composite fining upward successions (made of channel elements 5, 6 and 9) at the margin of channel complex 2 (Fig. 13). Composite fining upward successions for channel complex 1 are mainly located in the amalgamated channel axes (Fig. 13).

A potentially good analog for the relationship between vertical successions and stacking patterns of channel elements is from the Tres Pasos Formation, southern Chile (Reimchen et al., 2016). Both a vertical aggradation dominated stacking and a mixed lateral migration/vertical aggradation stacking are present in the Tres Pasos channel system (see Fig. 10 of Reimchen et al., 2016). Their measured sections and cross-sectional architecture are consistent with our interpretation above. Another potential analog comes from two sedimentological conceptual models based on subsurface datasets

(see Figs, 2, 3 of Labourdette, 2007). The corresponding wireline log motifs demonstrate the better-developed fining upward trend (a bell-shaped log motif) related to the lateral migration/vertical aggradation stacking pattern, compared to a cylindrical log motif at the stacked margins of the vertical aggradation dominated channel system (Labourdette, 2007).

### 9.3. Applications for hydrocarbon systems

Firstly, strong cross-channel facies architecture asymmetry has a significant effect on reservoir quality prediction. The axis of channel elements similar to those in the study area are dominated by better (higher net-to-gross, more vertically connected) reservoir facies than those of channel margins which feature poorer quality reservoir facies with the common presence of the silty drapes. Importantly, the two different types of drapes (bypass drapes and deposition drapes) are expected to exhibit different lateral extents and thus have different effects on fluid flow. Bypass drapes may extend from channel margins to the axis, whereas deposition drapes tend to transition towards the channel axis into reservoir facies. As a result, deposition drapes probably act as flow baffles, whereas bypass drapes could act as flow barriers and, therefore, have potentially different effects on the sweep efficiency and final hydrocarbon recovery (cf., Barton et al., 2010; Li and Caers, 2011; Alpak et al., 2013).

Secondly, stacking patterns of channel elements with asymmetric facies architecture that is below seismic resolution add to the complexity and uncertainty of reservoir heterogeneity. Due to the development of non-reservoir facies (silty drapes) at the inner bend, unidirectional lateral migration (e.g., channel elements 5-8) towards the outer bend likely results in the separation of successive channels by silty deposition drapes or bypass drapes at channel margins, and can result in reservoir compartmentalization (cf., Barton et al., 2010; Pyles et al., 2010; Funk et al., 2012; Alpak et al., 2013; Hubbard et al., 2014). The compartmentalization, however, could be significantly reduced due to erosion of heterogeneous marginal deposits when non-sequential stacking contacts exist (cf., Funk et al., 2012) (e.g., between channel elements 6 and 9, 7 and 9). In contrast, in the scenario of vertical aggradation of channel elements (e.g., channel elements 1-4); deposition drapes in the channel margin are less likely to affect the connectivity between two adjacent channel elements because channel axes are in contact. However, if bypass drapes are present and well preserved in the channel axis, then there is probably still no connectivity between the sands in two adjacent channel elements (cf., Labourdette, 2007; Labourdette and Bez, 2010; Funk et al., 2012).

Thirdly, these observations provide guidelines to well placement for hydrocarbon production in sinuous submarine channels with asymmetrical facies distributions. If producing wells are drilled in close proximity to outer bends where the coarse-grained channel axial facies dominates, early water breakthrough may occur (e.g., Stewart et al., 2008), leaving behind a significant amount of hydrocarbons closer to the heterogeneous inner bend. On the other hand, if wells are located too close to the inner bend margin, then they might encounter significant flow barriers and baffles such as bypass and deposition drapes (cf., Gardiner, 2006). This reduces or precludes production of the hydrocarbons within the thick sand bodies downdip toward the channel axis (cf., Gardiner, 2006).

## 10. Conclusions

The exposed Capistrano Formation at San Clemente, California, records nine stacked sandy submarine channel elements (200-400 m wide) with asymmetric cross-sectional facies architecture and low-sinuosity planform geometry. The best-exposed channel element (channel element 9) demonstrates that coarser-grained and thicker-bedded axis deposits are partitioned to the slightly steeper channel edge (presumed outer bend), whereas finer-grained, thinner bedded and less amalgamated channel margin dominate towards slightly gentler dipping (presumed inner bend) channel edge. Two different types of silty drapes (bypass drapes vs. deposition drapes) are recognized based on their different grain size ranges, lateral geometries, distributions, associated erosion/bypass features, and upward changes in bed dips (Table 2). They are attributed respectively to dilute muddy tails of bypassing flows and depositional flows that deposited axial sands and marginal silty drapes contemporaneously.

The nine channel elements make up two channel complexes that show two commonly observed submarine channel stacking patterns (a vertical aggradation stacking vs. a mixed lateral migration/vertical aggradation stacking). The two different patterns of channel stacking dictate variable preservation of channel elements, which in turn affect their vertical profiles. For channels with a mixed lateral migration/vertical aggradation stacking, composite fining upward successions are expected to be best developed at the inner bank. In contrast, for channels with a vertical aggradation stacking, well-defined composite fining upward successions tend to occur in the channel axis of the composite channel.

Asymmetric facies architecture and different types of drapes within channel elements, their relationship with channel planform geometry, as well as the stacking patterns of channel elements

have significant implications for hydrocarbon development and production in terms of reservoir heterogeneity and compartmentalization.

### **Acknowledgements**

This work comprised part of the doctoral studies of PL and part of the Joint Industry Project, PRACSS, which was funded by BG Group, BP, DONG, RWE Dea, Petrochina, Statoil and Tullow Oil. PL also acknowledges the China Scholarship Council (CSC) for providing a stipend for his Ph.D. study in the UK. We are grateful to Guilherme Bozetti and Dugmar Isabel Mendez for their assistance in the field. We wish to thank Lana Nguyen, Dennis Weber, Christina Donehower and others from the state park for sample and work permission. We are also indebted to Christopher J. Stevenson, the anonymous reviewer and the editor Jasper Knight for their constructive and thoughtful reviews that improved the clarity and focus of manuscript considerably.

### **References**

- Abreu, V., Sullivan, M., Pirmez, C., Mohrig, D., 2003. Lateral accretion packages (LAPs): an important reservoir element in deep water sinuous channels. *Marine and Petroleum Geology* 20, 631–648.
- Alpak, F.O., Barton, M.D., Naruk, S.J., 2013. The impact of fine-scale turbidite channel architecture on deepwater reservoir performance. *AAPG Bulletin* 97, 251-284.
- Arnott, R.W.C., 2007. Stratal architecture and origin of lateral accretion deposits (LADs) and conterminous inner-bank levee deposits in a base-of-slope sinuous channel, lower Isaac Formation (Neoproterozoic), East-Central British Columbia, Canada. *Marine and Petroleum Geology* 24, 515–528.
- Babonneau, N., Savoye, B., Cremer, M., Klein, B., 2002. Morphology and architecture of the present canyon and channel system of the Zaire deep-sea fan. *Marine and Petroleum Geology* 19, 445–467.
- Babonneau, N., Savoye, B., Cremer, M., Bez, M., 2004. Multiple terraces within the deep incised Zaire Valley (ZaiAngo Project): are they confined levees? In: Lomas, S.A., Joseph, P. (Eds.), *Confined Turbidite Systems*. Geological Society of London, Special Publications 222, pp. 91–114.
- Babonneau, N., Savoye, B., Cremer, M., Bez, M., 2010. Sedimentary architecture in meanders of a submarine channel: detailed study of the present Congo turbidite channel (Zaiango project). *Journal of Sedimentary Research* 80, 852–866.

- Bain, H.A., Hubbard, S.M., 2016. Stratigraphic evolution of a long-lived submarine channel system in the Late Cretaceous Nanaimo Group, British Columbia, Canada. *Sedimentary Geology* 337, 113–132.
- Barton, M., O'Byrne, C., Pirmez, C., Prather, B., Vlugt, F. Van Der, Alpak, F.O., Sylvester, Z., 2010. Turbidite channel architecture: recognizing and quantifying the distribution of channel-base drapes using core and dipmeter data. In: Pöppelreiter, M., García-Carballido, C., Kraaijeveld, M.A. (Eds.), *Dipmeter and Borehole Image Log Technology*. AAPG Memoir 92, pp. 195–210.
- Beaubouef, R.T., Rossen, C., Zelt, F.B., Sullivan, M.D., Mohrig, D.C., Jennette, D.C., 1999. Deep-water sandstones, Brushy Canyon Formation, West Texas. *American Association of Petroleum Geologists, Continuing Education Course Notes* 40, 1–50.
- Bouma, A.H., 1962. *Sedimentology of Some Flysch Deposits: A Graphic Approach to Facies Interpretation*. Elsevier, Amsterdam, 168 pp.
- Bouroullec, R., David, R.P., Daniel, E.S., David, C.J., Bonnaffé, F., 2007. Impact of local accommodation on the architecture and stacking patterns of three Capistrano Formation slope channel outcrops: San Clemente, Dana Point Harbor and Point Fermin, California. *AAPG Annual Meeting Abstracts*, Long Beach, California, pp. 15-18.
- Bouroullec, R., Pyles, D.R., 2010. Sandstone extrusions and slope channel architecture and evolution: Mio-Pliocene Monterey and Capistrano Formations, Dana Point Harbor, Orange County, California, U.S.A. *Journal of Sedimentary Research* 80, 376–392.
- Busby, C.J., Camacho, H., Kneller, B., 1998. A new model for the Miocene-Pliocene turbidite system at San Clemente, CA (abs.). *AAPG Bulletin* 82, 844.
- Callow, R.H.T., Kneller, B., Dykstra, M., McIlroy, D., 2014. Physical, biological, geochemical and sedimentological controls on the ichnology of submarine canyon and slope channel systems. *Marine and Petroleum Geology* 54, 144–166.
- Camacho, H., Busby, C.J., Kneller, B., 2002. A new depositional model for the classical turbidite locality at San Clemente State Beach, California. *AAPG Bulletin* 86, 1543–1560.
- Campion, K.M., Sprague, A.R., Mohrig, D., Lovell, R.W., Drzewiecki, P.A., Ardill, J.A., Jensen, G.N., Sickafoose, D.K., 2000. Outcrop expression of confined channel complexes. In: Weimer, P.,

- Slatt, R.M., Coleman, J.L., Rosen, N., Nelson, C.H., Bouma, A.H., Styzen, M., Lawrence, D.T. (Eds.), Deep-Water Reservoirs of the World. GCSSEPM Foundation 20th Annual Research Conference, pp. 127–151.
- Campion, K.M., Sprague, A.R., Sullivan, M.D., 2005. Architecture and lithofacies of the Capistrano Formation (Miocene-Pliocene), San Clemente, California. AAPG Fieldtrip Guidebook 100, SEPM, Fullerton Pacific Section, Fullerton, California, pp. 1-42.
- Campion, K.M., Sprague, A.R., Sullivan, M.D., 2007. Architecture and lithofacies of the Miocene Capistrano Formation, San Clemente State Beach, California, U.S.A. In: Nilsen, T.H., Shew, R.D., Steffens, G.S., Studlick, J.R.J. (Eds.), Atlas of Deep-water Outcrops. AAPG Studies in Geology 56, pp. 395–400.
- Chapin, M., Keller, F., 2007. Channel-fill sandstones at San Clemente State Beach, California, USA. In: Nilsen, T.H., Shew, R.D., Steffens, G.S., Studlick, J.R.J. (Eds.), Atlas of Deep-water Outcrops. AAPG Studies in Geology 56, pp. 401–405.
- Clark, J.D., Pickering, K.T., 1996. Architectural elements and growth patterns of submarine channels: application to hydrocarbon exploration. AAPG Bulletin 80, 194–221.
- Cross, N.E., Cunningham, A., Cook, R.J., Taha, A., Esmatie, E., El Swidan, N., 2009. Three-dimensional seismic geomorphology of a deep-water slope-channel system: The Sequoia field, offshore west Nile Delta, Egypt. AAPG Bulletin 93, 1063–1086.
- Deptuck, M.E., Steffens, G.S., Barton, M., Pirmez, C., 2003. Architecture and evolution of upper fan channel-belts on the Niger Delta slope and in the Arabian Sea. Marine and Petroleum Geology 20, 649–676.
- Deptuck, M.E., Sylvester, Z., Pirmez, C., O'Byrne, C., 2007. Migration–aggradation history and 3-D seismic geomorphology of submarine channels in the Pleistocene Benin-major Canyon, western Niger Delta slope. Marine and Petroleum Geology 24, 406–433.
- De Ruig, M.J., Hubbard, S.M., 2006. Seismic facies and reservoir characteristics of a deep-marine channel belt in the Molasse foreland basin, Puchkirchen Formation, Austria. AAPG Bulletin 90, 735–752.
- Ehlig, P., 1979. The late Cenozoic evolution of the Capistrano Embayment. In: Fife, D.L. (Ed.), Geology guide to San Onofre Nuclear Station and adjacent regions of Southern California, Pacific sections. American Association of Petroleum Geologists, SEPM, and Society of

- Exploration Geophysicists, pp. 38–46.
- Elliott, T., 2000. Megaflute erosion surfaces and the initiation of turbidite channels. *Geology* 28, 119–122.
- Fildani, A., Hubbard, S.M., Covault, J.A., Maier, K.L., Romans, B.W., Traer, M., Rowland, J.C., 2013. Erosion at inception of deep-sea channels. *Marine and Petroleum Geology* 41, 48–61.
- Funk, J.E., Slatt, R.M., Pyles, D.R., 2012. Quantification of static connectivity between deep-water channels and stratigraphically adjacent architectural elements using outcrop analogs. *AAPG Bulletin* 96, 277–300.
- Gamberi, F., Dykstra, M., Kane, I.A., Kneller, B.C., 2013. Integrating modern seafloor and outcrop data in the analysis of slope channel architecture and fill. *Marine and Petroleum Geology* 41, 83–103.
- Gardiner, A.R., 2006. The variability of turbidite sandbody pinchout and its impact on hydrocarbon recovery in stratigraphically trapped fields. In: Allen, M.R., Goffey, G.P., Morgan, R.K., Walker, I.M. (Eds.), *The Deliberate Search for the Stratigraphic Trap*. Geological Society of London, Special Publications 254, pp. 267–287.
- Gardner, M.H., Borer, J.M., Melick, J.J., Mavilla, N., Dechesne, M., Wagerle, R.N., 2003. Stratigraphic process-response model for submarine channels and related features from studies of Permian Brushy Canyon outcrops, West Texas. *Marine and Petroleum Geology* 20, 757–787.
- Grecula, M., Flint, S.S., Wickens, H.D., Johnson, S.D., 2003. Upward-thickening patterns and lateral continuity of Permian sand-rich turbidite channel fills, Laingsburg Karoo, South Africa. *Sedimentology* 50, 831–853.
- Hansen, L.A.S., Callow, R.H.T., Kane, I.A., Gamberi, F., Rovere, M., Cronin, B.T., Kneller, B.C., 2015. Genesis and character of thin-bedded turbidites associated with submarine channels. *Marine and Petroleum Geology* 67, 852–879.
- Hein, F.J., Walker, R.G., 1982. The Cambro-Ordovician Cap Enrage Formation, Quebec, Canada: conglomeratic deposits of a braided submarine channel with terraces. *Sedimentology* 29, 309–352.



- Hess, G.R., 1979. Miocene and Pliocene inner suprafan channel complex, San Clemente, California. In: Stuart, C.J. (Ed.), Guidebook to Miocene Lithofacies & Depositional Environments, Coastal Southern California & Northwestern Baja California. SEPM Pacific Section, Los Angeles, California, pp.99–106.
- Hickson, T.A., Lowe, D.R., 2002. Facies architecture of a submarine fan channel–levee complex: the Juniper Ridge Conglomerate, Coalinga, California. *Sedimentology* 49, 335–362.
- Hodgson, D.M., Di Celma, C.N., Brunt, R.L., Flint, S.S., 2011. Submarine slope degradation and aggradation and the stratigraphic evolution of channel–levee systems. *Journal of the Geological Society of London* 168, 625–628.
- Hodgson, D.M., Kane, I.A., Flint, S.S., Brunt, R.L., Ortiz-Karpf, A., 2016. Time-transgressive confinement on the slope and the progradation of basin-floor fans: implications for the sequence stratigraphy of deep-water deposits. *Journal of Sedimentary Research* 86, 73–86.
- Hubbard, S.M., Covault, J.A., Fildani, A., Romans, B.W., 2014. Sediment transfer and deposition in slope channels: deciphering the record of enigmatic deep-sea processes from outcrop. *Geological Society of America Bulletin* 126, 857–871.
- Ingle, J.C., 1971. Paleoecologic and paleobathymetric history of the Late Miocene–Pliocene Capistrano Formation, Dana Point area, Orange County, California. In: Bergen, F.W. (Ed.), Geologic guidebook, Newport Lagoon to San Clemente, California. SEPM Pacific Section, pp. 55–70.
- Janocko, M., Nemeč, W., Henriksen, S., Warchoł, M., 2013. The diversity of deep-water sinuous channel belts and slope valley-fill complexes. *Marine and Petroleum Geology* 41, 7–34.
- Jester, T.R., 2013. Controls on submarine channel architecture, Upper Miocene–Lower Pliocene Capistrano Formation, San Clemente State Beach, California. Master thesis, Montana State University, 153 pp.
- Jobe, Z.R., Bernhardt, A., Lowe, D.R., 2010. Facies and architectural asymmetry in a conglomerate-rich submarine channel fill, Cerro Toro Formation, Sierra Del Toro, Magallanes Basin, Chile. *Journal of Sedimentary Research* 80, 1085–1108.

- Kane, I.A., Kneller, B.C., Dykstra, M., Kassem, A., McCaffrey, W.D., 2007. Anatomy of a submarine channel–levee: an example from Upper Cretaceous slope sediments, Rosario Formation, Baja California, Mexico. *Marine and Petroleum Geology* 24, 540–563.
- Kane, I.A., Dykstra, M.L., Kneller, B.C., Tremblay, S., McCaffrey, W.D., 2009. Architecture of a coarse-grained channel–levée system: the Rosario Formation, Baja California, Mexico. *Sedimentology* 56, 2207–2234.
- Kneller, B.C., Branney, M.J., 1995. Sustained high-density turbidity currents and the deposition of thick massive sands. *Sedimentology* 42, 607–616.
- Kolla, V., Bandyopadhyay, A., Gupta, P., Mukherjee, B., Ramana, D.V., 2012. Morphology and internal structure of a recent upper Bengal fan-valley complex. In: Prather, B.E., Deptuck, M.E., Mohrig, D., Van Hoorn, B., Wynn, R.B. (Eds.), *Application of the Principles of Seismic Geomorphology to Continental Slope and Base of Slope Systems: Case Studies from Seafloor and Near-Seafloor Analogues*. SEPM Special Publication 99, pp. 347–369.
- Labourdette, R., 2007. Integrated three-dimensional modeling approach of stacked turbidite channels. *AAPG Bulletin* 91, 1603–1618.
- Labourdette, R., Bez, M., 2010. Element migration in turbidite systems: random or systematic depositional processes? *AAPG Bulletin* 94, 345–368.
- Li, H., Caers, J., 2011. Geological modeling and history matching of multiscale flow barriers in channelized reservoirs: methodology and application. *Petroleum Geoscience* 17, 17–34.
- Lien, T., Walker, R.G., Martinsen, O.J., 2003. Turbidites in the Upper Carboniferous Ross Formation, Western Ireland: reconstruction of a sinuous channel and sandy spillover system. *Sedimentology* 50, 113–148.
- Lowe, D.R., 1982. Sediment gravity flows: II. Depositional models with special reference to the deposits of high-density turbidity currents. *Journal of Sedimentary Petrology* 52, 279–297.
- Macauley, R.V., Hubbard, S.M., 2013. Slope channel sedimentary processes and stratigraphic stacking, Cretaceous Tres Pasos Formation slope system, Chilean Patagonia. *Marine and Petroleum Geology* 41, 146–162.

- Maier, K.L., Fildani, A., McHargue, T.R., Paull, C.K., Graham, S.A., Caress, D.W., 2012. Punctuated deep-water channel migration: high-resolution subsurface data from the Lucia Chica channel system, offshore California, U.S.A. *Journal of Sedimentary Research* 82, 1–8.
- Malone, N.J., Alba, C.A., 1979. Marine fan-channel facies of upper Miocene Capistrano Formation, San Clemente, California. In: Keaton, J.R. (Ed.), *Guidebook to Selected Geological Features: Coastal Areas of Southern Orange and Northern San Diego Counties, California*. pp. 77–89.
- Mayall, M., Lonergan, L., Bowman, A., James, S., Mills, K., Primmer, T., Pope, D., Rogers, L., Skeene, R., 2010. The response of turbidite slope channels to growth-induced seabed topography. *AAPG* 94, 1011–1030.
- McHargue, T., Pyrcz, M.J., Sullivan, M.D., Clark, J.D., Fildani, A., Romans, B.W., Covault, J.A., Levy, M., Posamentier, H.W., Drinkwater, N.J., 2011. Architecture of turbidite channel systems on the continental slope: patterns and predictions. *Marine and Petroleum Geology* 28, 728–743.
- Mutti, E., Normark, W.R., 1987. Comparing examples of modern and ancient turbidite systems: problems and concepts. In: Legett, J.K., Zuffa, G.G. (Eds.), *Marine Clastic Sedimentology: Concepts and Case Studies*. Graham and Trotman, London, pp. 1–38.
- Mutti, E., 1992. *Turbidite Sandstones*. San Donato, Milanese, Università di Parma, Agip, 275 pp.
- Paull, C.K., Caress, D.W., Ussler III, W., Lundstern, E., Meiner-Johnson, M., 2011. High-resolution bathymetry of the axial channels within Monterey and Soquel submarine canyons, offshore central California. *Geosphere* 7, 1077–1101.
- Paull, C.K., Caress, D.W., Lundstern, E., Gwiazda, R., Anderson, K., McGann, M., Conrad, J., Edwards, B., Sumner, E.J., 2013. Anatomy of the La Jolla Submarine Canyon system; offshore southern California. *Marine Geology* 335, 16–34.
- Peakall, J., McCaffrey, B., Kneller, B., 2000. A process model for the evolution, morphology, and architecture of sinuous submarine channels. *Journal of Sedimentary Research* 70, 434–448.
- Pickering, K.T., 1982. Middle-fan deposits from the late Precambrian Kongsfjord formation submarine fan, Northeast Finnmark, Northern Norway. *Sedimentary Geology* 33, 79–110.
- Pickering, K., Coleman, J., Cremer, M., Droz, L., Kohl, B., Normark, W., O'Connell, S., Stow, D., Meyer-Wright, A., 1986. A high sinuosity, laterally migrating submarine fan channel-levee-overbank: results from DSDP Leg 96 on the Mississippi Fan, Gulf of Mexico. *Marine and*

- Petroleum Geology 3, 3–18.
- Pickering, K.T., Hiscott, R.N., 2016. Deep marine systems: processes, deposits, environments, tectonics and sedimentation. John Wiley & Sons, Chichester, West Sussex, UK; Hoboken, New Jersey, USA, 657 pp.
- Posamentier, H.W., Walker, R.G., 2006. Deep-water turbidites and submarine fans. In: Posamentier, H.W., Walker, R.G. (Eds.), *Facies Models Revisited*. SEPM Special Publication 84, pp. 399-520.
- Pyles, D.R., Jennette, D.C., Tomasso, M., Beaubouef, R.T., Rossen, C., 2010. Concepts learned from a 3D outcrop of a sinuous slope channel complex: Beacon Channel Complex, Brushy Canyon Formation, West Texas, U.S.A. *Journal of Sedimentary Research* 80, 67–96.
- Reimchen, A.P., Hubbard, S.M., Stright, L., Romans, B.W., 2016. Using sea-floor morphometrics to constrain stratigraphic models of sinuous submarine channel systems. *Marine and Petroleum Geology* 77, 92–115.
- Sprague, A.R., Sullivan, M.D., Campion, K.M., Jensen, G.N., Goulding, F.J., Garfield, T.R., Sickafoose, D.K., Rossen, C., Jennette, D.C., Beaubouef, R.T., Abreu, V., Ardill, J., Porter, M.L., Zelt, F.B., 2002. The physical stratigraphy of deep-water strata: a hierarchical approach to the analysis of genetically related stratigraphic elements for improved reservoir prediction. AAPG Annual Meeting Abstracts, Houston, pp. 10-13.
- Sprague, A.R.G., Garfield, T.R., Goulding, F.J., Beaubouef, R.T., Sullivan, M.D., Rossen, C., Campion, K.M., Sickafoose, D.K., Abreu, D., Schellpeper, M.E., Jensen, G.N., Jennette, D.C., Pirmez, C., Dixon, B.T., Ying, D., Ardill, J., Mohrig, D.C., Porter, M.L., Farrell, M.E., Mellere, D., 2005. Integrated slope channel depositional models: the key to successful prediction of reservoir presence and quality in offshore West Africa, CIPM, cuarto E-Exitep. Veracruz, Mexico, pp. 1-13.
- Stelling, C.E., DSDP Leg 96 Shipboard Scientists, 1985. Migratory characteristics of a mid-fan meander belt, Mississippi Fan. In: Bouma, A.H., Barnes, N.E., Normark, W.R. (Eds.), *Submarine Fans and Related Turbidite Sequences*. New York, Springer-Verlag, pp. 283–290.
- Stevenson, C.J., Talling, P.J., Sumner, E.J., Masson, D.G., Frenz, M., Wynn, R.B., 2014. On how thin submarine flows transported large volumes of sand for hundreds of kilometres across a flat basin plain without eroding the sea floor. *Sedimentology* 61, 1982–2019.

- Stevenson, C.J., Jackson, C.A.-L., Hodgson, D.M., Hubbard, S.M., Eggenhuisen, J.T., 2015. Deep-water sediment bypass. *Journal of Sedimentary Research* 85, 1058–1081.
- Stewart, J., Dunn, P., Lyttle, C., Campion, K., Oyerinde, A., 2008. Improving performance prediction in deep-water reservoirs: learning from outcrop analogues, conceptual models and flow simulation. *International Petroleum Technology Conference, Malaysia*, pp. 1–9.
- Straub, K.M., Mohrig, D., McElroy, B., Buttles, J., Pirmez, C., 2008. Interactions between turbidity currents and topography in aggrading sinuous submarine channels: a laboratory study. *Geological Society of America Bulletin* 120, 368–385.
- Strong, N., Paola, C., 2008. Valleys that never were: time surfaces versus stratigraphic surfaces. *Journal of Sedimentary Research* 78, 579–593.
- Sullivan, M., Jensen, G., Goulding, F., Jennette, D., Foreman, L., Stern, D., 2000. Architectural analysis of deep-water outcrops: implications for exploration and development of the Diana sub-basin, western Gulf of Mexico. In: Weimer, P., Slatt, R.M., Coleman, J., Rosen, N.C., Nelson, H., Bouma, A.H., Styzen, M.J., Lawrence, D.T. (Eds.), *Deep-Water Reservoirs of the World*. GCSSEPM Foundation 20th Annual Research Conference, pp. 1010–1031.
- Sylvester, Z., Pirmez, C., Cantelli, A., 2011. A model of submarine channel–levee evolution based on channel trajectories: implications for stratigraphic architecture. *Marine and Petroleum Geology* 28, 716–727.
- Talling, P.J., Masson, D.G., Sumner, E.J., Malgesini, G., 2012. Subaqueous sediment density flows: depositional processes and deposit types. *Sedimentology* 59, 1937–2003.
- Walker, R.G., 1966. Deep channels in turbidite-bearing formations. *AAPG Bulletin* 50, 1899–1917.
- Walker, R.G., 1975. Nested submarine-fan channels in the Capistrano Formation, San Clemente, California. *Geological Society of America Bulletin* 86, 915–924.
- Weser, O.E., 1971. Proximal turbidite environment, San Clemente State Park. In: Bergen, F.W. (Eds.), *Geologic Guidebook, Newport Lagoon to San Clemente, California*. SEPM Pacific Section, Tulsa, Oklahoma, pp. 55–70.
- White, W.R., 1956. Pliocene and Miocene foraminifera from the Capistrano Formation, Orange

County, California. *Journal of Paleontology* 30, 237–260.

White, W.R., 1971. Biostratigraphy of the Capistrano Formation, Dana Point, Capistrano Beach area, California. In: Bergen, F.W. (Ed.), *Geologic Guidebook, Newport Lagoon to San Clemente, California: Coastal Exposures of Miocene and Early Pliocene Rocks*. SEPM Pacific Section, Tulsa, Oklahoma, pp. 50–54.

**Table 1. Characterization of facies within the Capistrano Formation slope channel system exposed at San Clemente (see Fig. 4 for representative photos).**

**Table 2. Recognition criteria, formative mechanisms, and time equivalent sands of bypass drapes and deposition drapes based on the outcrop at San Clemente.**

**Table 3. Paleoflow measurements and channel edge trends at San Clemente.**

## Figure Captions

Fig. 1. (a) Map showing the location and paleogeography of the study area with the Capistrano Embayment highlighted (modified from Ehlig, 1979). (b) Map of the study area showing the three primary sections of this study (sections A-C).

Fig. 2. Generalized stratigraphic column for Dana Point and the study area at San Clemente (modified from Campion et al., 2005; Bouroullec and Pyles, 2010; Jester, 2013).

Fig. 3. Schematic diagram showing the architectural hierarchy used in this study (modified from Campion et al., 2000, 2005; Sprague et al., 2002, 2005). The diagram (from top to bottom) presents channel architectural elements in increasing scales from facies to channel complex set. Facies are the building blocks that stack up to form channel elements with distinct sub-environments, including channel axis and channel margin. Two or more channel elements are nested to form a channel complex. Multiple channel complexes in turn stack up to form a channel complex set. Note the asymmetric cross-sectional profile of channel elements used in this modified hierarchical scheme.

Fig. 4. Representative photographs of sedimentary facies summarized in Table 1. (a) F1: bedded siltstone with faint parallel lamination and bioturbation (b) F2: silt-rich thin-bedded deposits; note sand injection from overlying and underlying massive sand of F4. (c) F3: sand-rich thin-bedded deposits. Note the supercritical climbing ripples indicating paleoflow towards the left. (d) F4: medium-to thick bedded sandstone, showing the common presence of loading structures. (e) F4: medium- to thick-bedded sandstone, showing the rare presence of a bar-like feature (highlighted with dashed lines) and more common massive sandstone with mudstone clasts. (f) F5: thin- to thick-bedded conglomerate. Measuring tape is circled for scale. (g) F6-a: mudstone-clast-rich conglomerate, showing the angular and disorganized mudstone-clasts. (h) F6-b: mudstone-clast-rich sandstone,

showing better sorting, rounding, and organization of mudstone-clasts than those in F6-a, and their association with parallel laminations.

Fig. 5. Photomosaic and interpretation of the turbidite slope channels of the Capistrano Formation exposed at San Clemente. (a) Overview photomosaic and interpretation of sections A-C. (b) Location map of sections A-C (see also Fig. 1), and legend used in this figure. (c-e) Detailed photomosaic and interpretation of sections A-C. Note the reference level (the horizontal axis) used here and below is the railroad track, as with Walker (1975), but the reference point of the horizontal axis is the northern end of section C in this study, which is approximately 350 m to the north of the reference point used in Walker (1975). See Fig. 3 for the schematic illustration of sub-environments within channel elements (i.e., channel axis, channel margin).

Fig. 6. Correlation panel of channel element 9 from its southern edge to northern edge. Note the characteristic asymmetry of facies architecture with channel axis facies located towards the northern edge, while channel margin with tabular deposits (terrace deposits or channel back-filling deposits) occurs towards the southern edge. See Fig. 5 for locations of the measured sections and, Fig. 9 and section 6.2 for interpretation. See Fig. 5 for key to the colors used.

Fig. 7. Lateral variations within channel element 9. (a) Medium-to thick-bedded sandy and conglomeratic channel axis deposits dominate at its northern edge. (b) Interbedded medium-to thick-bedded sandstone and thin-bedded heterolithic deposits characterize the intra-channel tabular units (highlighted with an arrow). (c) Low-relief, intra-channel erosional surface (highlighted with black arrows) are locally draped by thin-bedded heterolithic deposits at channel margin. (d) Panoramic view of the southern margin of channel element 9. See Fig. 6 for more details of the bed packages (indicated by circled numbers) and the measured section (MS15). Note the more gentle inclination of the southern edge than the northern counterpart in (a). (e-f) Uninterpreted, enlarged view and interpreted line drawing of the outlined area in part D, showing the transition of sand and thin beds into silty drapes in close proximity to the southern edge of channel element 9.



Fig. 8. (a) Graph showing lateral thickness variations of packages 2-5 within channel element 9. Notice the irregular geometry of package 2, the wedge-shaped geometry of package 3, and the tabular geometry of packages 4 and 5 in cross section. (b) Graph showing lateral thickness variations of individual sandstone beds within package 2 of channel element 9. Notice abrupt lateral changes in bed thickness at MS21 and MS18, where local scours are present at the base of package 2. See Fig. 6 for the corresponding correlation panel for the plots in (a) and (b). The reference point referred to is the northern end of section C (see Fig. 5).

Fig. 9. (a) Schematic illustration of the architecture model of channel elements at San Clemente (based partially on McHargue et al., 2011). Note the distribution of sub-channel elements, including channel axis, channel margin with tabular deposits (interpreted as terrace deposits or channel back-filling deposits), as well as associated silty drapes. (b) Bed packages, and locations of representative outcrop examples shown in other figures, illustrating different parts of the architecture model.

Fig. 10. Outcrop characteristics of bypass drapes and deposition drapes. (a) Photomosaic showing the stepped profiles of channel edges of channel elements 2 and 3 (CE 2 and 3). (b) Interpretive line drawing of (a). Intra-channel bypass drapes overlie nearly horizontal erosional surfaces within channel element 3 (CE 3). A deposition drape overlies the channel edge of channel element 2, showing a convergent shape; also note the tabular deposits of CE 2; (c) A bypass drape overlies the channel edge of channel element 4 (CE 4). Note the scale (indicated by a yellow outline) is about 40cm long. (d) Close-up of the channel-base bypass drape in C. Note the ripped-up sandstone clast at the base of the drape. See Fig. 5 for key to colors used in (b), and section 6.2.3 for detailed discussion of bypass drapes and deposition drapes.

Fig. 11. Cartoons illustrating cross-channel depositional processes in two different scenarios for depositing silty drapes (modified from Stevenson et al., 2014). (a) Flow is very erosive and bypassing, resulting in mudstone-clast-rich conglomerates or coarse-grained residual lags by the head and body of the flow, as well as the formation of a silty drape (termed bypass drape) by the tail. (b) Flow is depositional and is characterized by contemporaneous deposition of a silty drape (termed deposition

draped) at the channel margin (higher) and sand towards the channel axis (lower) due to the stratification of the flow.

Fig. 12. Cartoons illustrating stacking pattern interpretation based on 2D partial exposure in outcrop. Either a vertical aggradation stacking pattern (a) or a lateral migration stacking pattern (b) can give rise to a similar 2D geometry in outcrop (marked by the red boxes), highlighting the pitfalls of reconstruction of stacking patterns based solely on limited 2D geometries.

Fig. 13. Cartoon showing the inferred stacking patterns of channel elements within each of the two channel complexes. Channel elements 1-4 (CE 1-4) belonging to channel complex 1, are dominated by vertical aggradation, whilst channel elements 5-9 (CE 5-9) belonging to channel complex 2, show mixed lateral migration/vertical aggradation. Note the exposures examined in this study (highlighted with the red box) represent only a thin slice through a much larger channel system, most of which is inferred to be buried in the subsurface and above the present exposure.

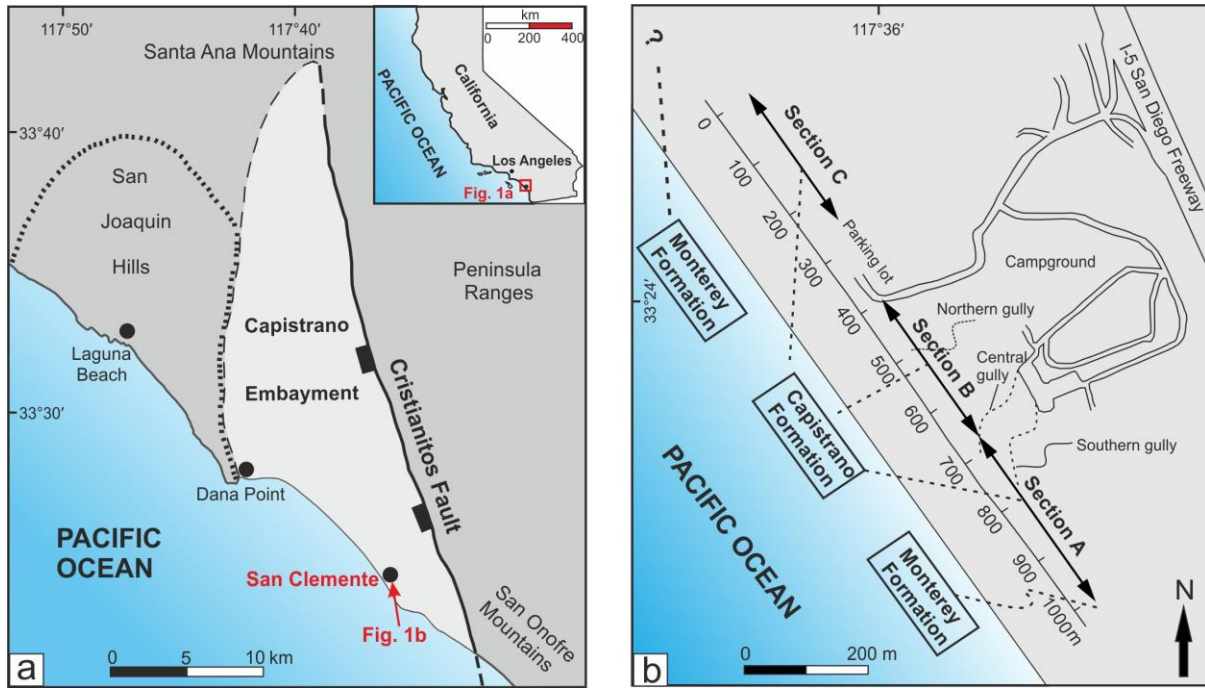


Figure 1

Approximate thickness	Lithostratigraphy	Age	Stratigraphic unit	Description and interpretation	
45 m		Pleistocene	Terrace Deposit	Mainly sandstone (marine terrace) unconformity	
		Pliocene	<b>Capistrano Formation</b>	Mainly sandstone and conglomerate at San Clemente State Beach (study area) and Dana Point Only around 15 m of the Capistrano Formation exposed in the study area (deep-marine channel fills and slope deposits) unconformity	
525 m		Upper			
250 m		Miocene	Middle	Monterey Formation	Predominately shale and siltstone with subordinate sandstone (deep marine setting) unconformity
1400 m				San Onofre Breccia	Sandstone and Conglomerate (shallow marine setting)

Figure 2

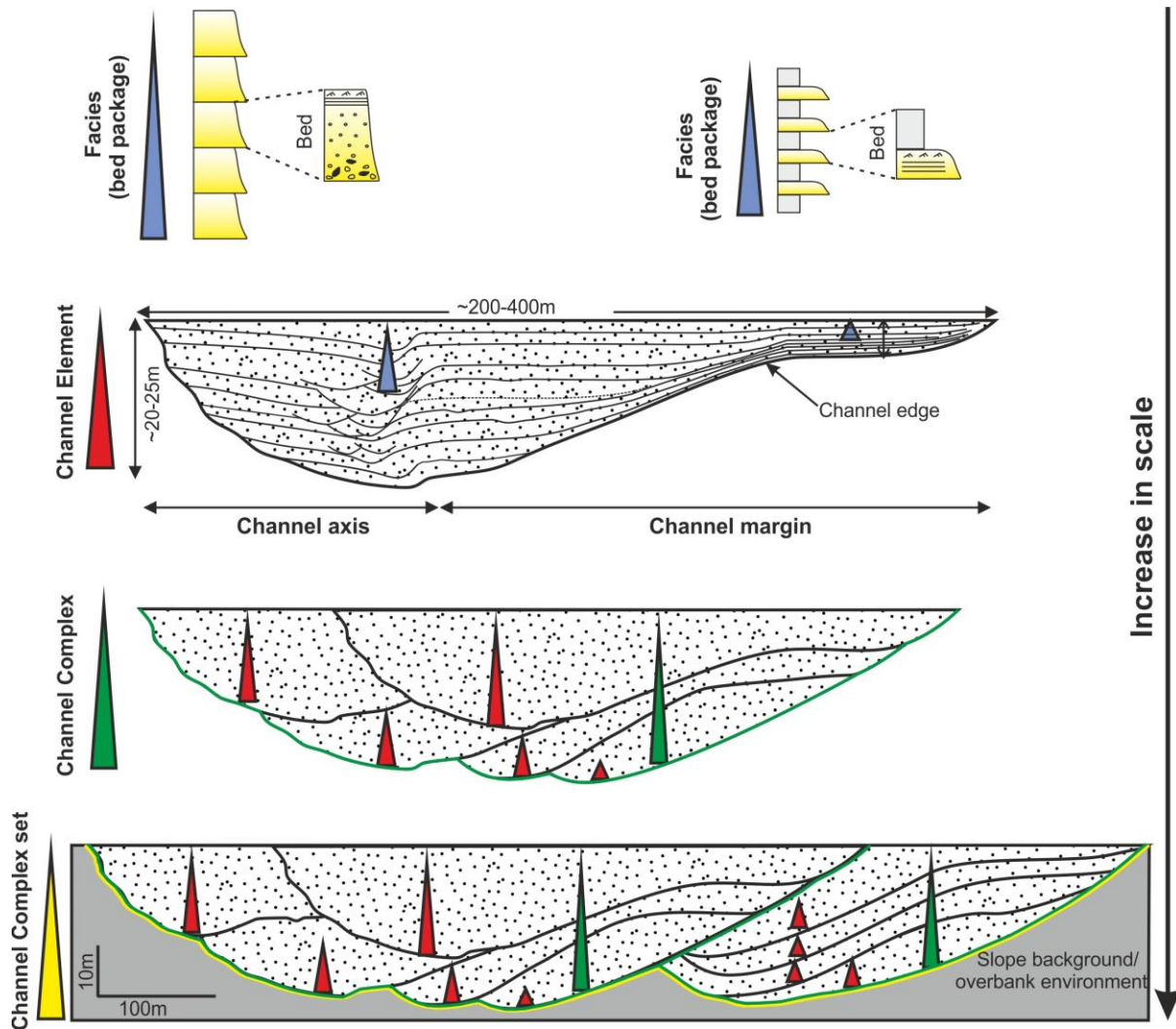


Figure 3



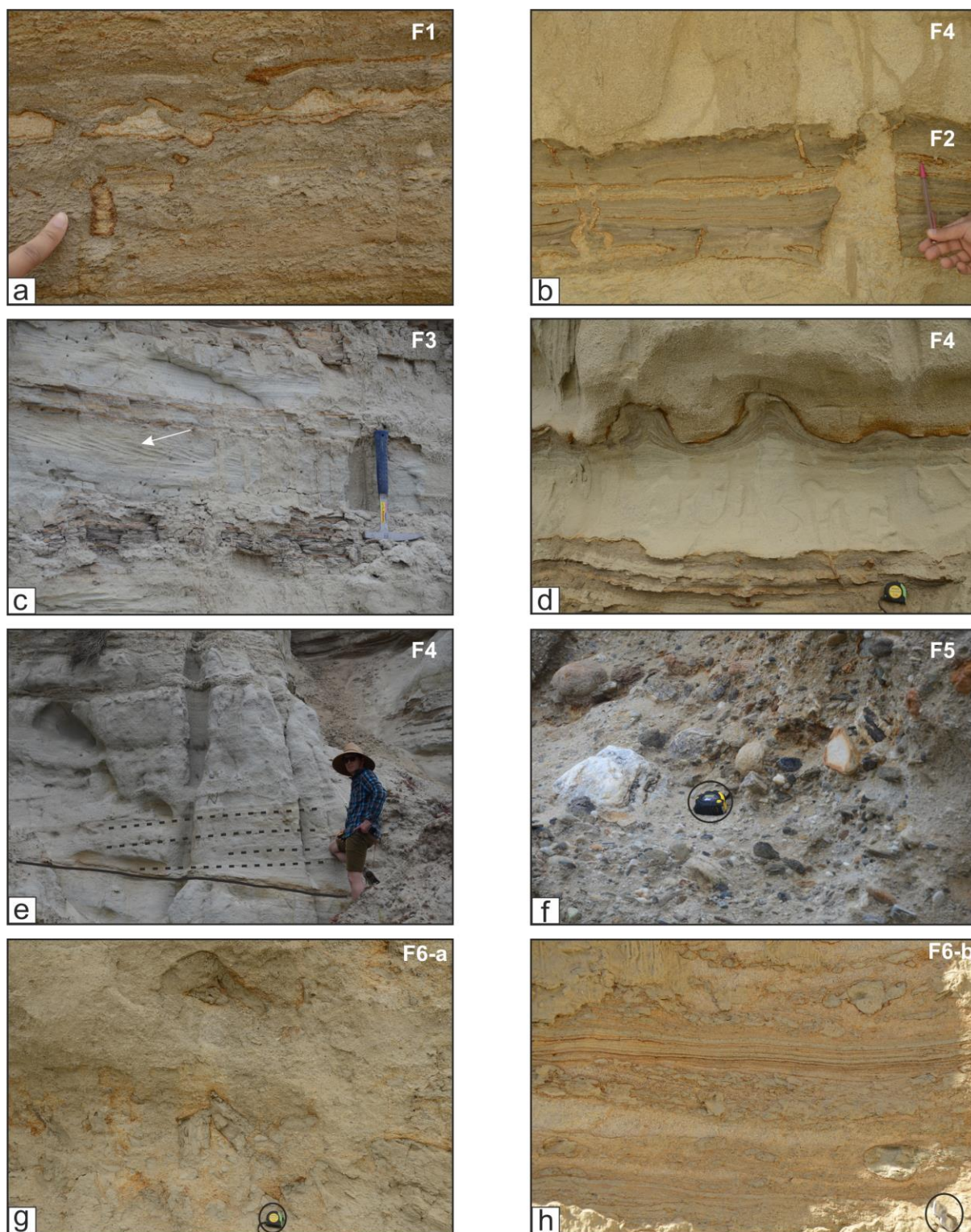


Figure 4

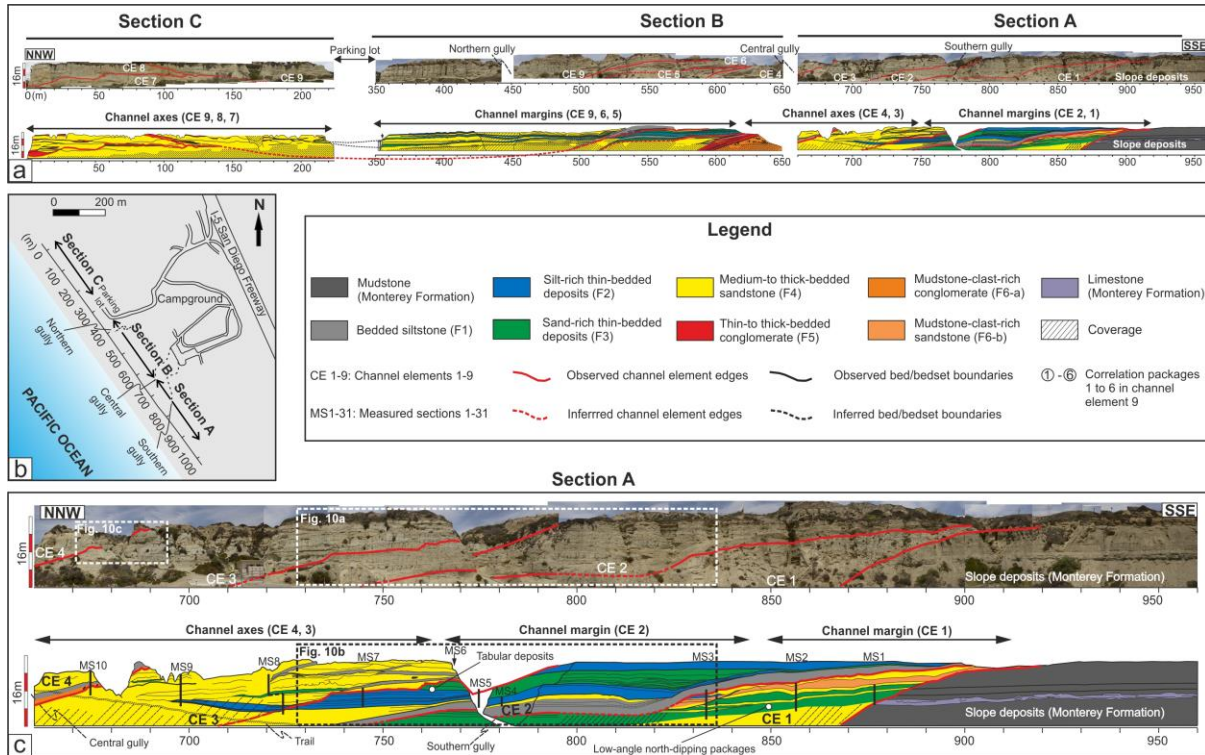


Figure 5abc

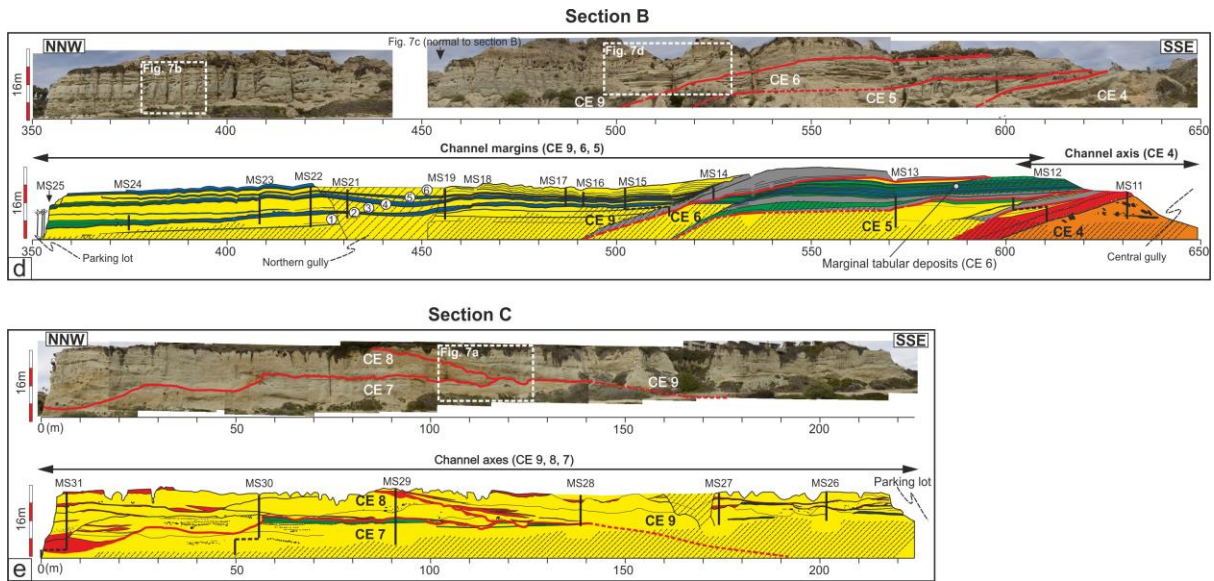


Figure 5de



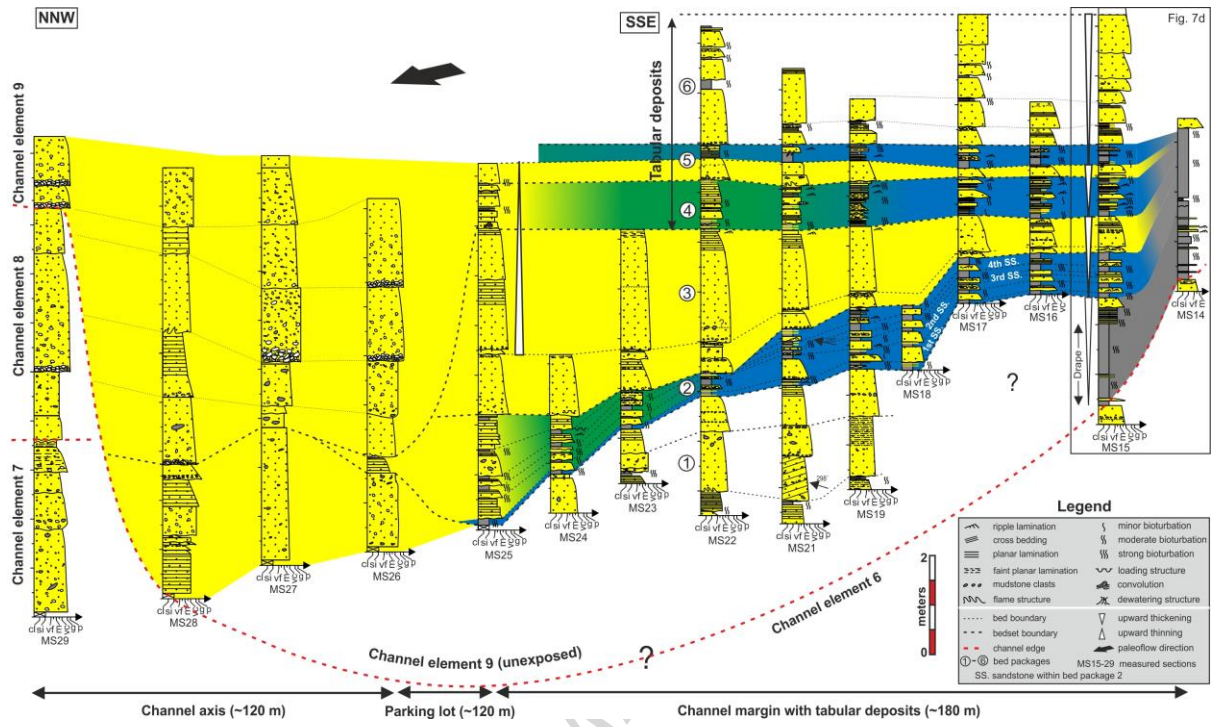


Figure 6

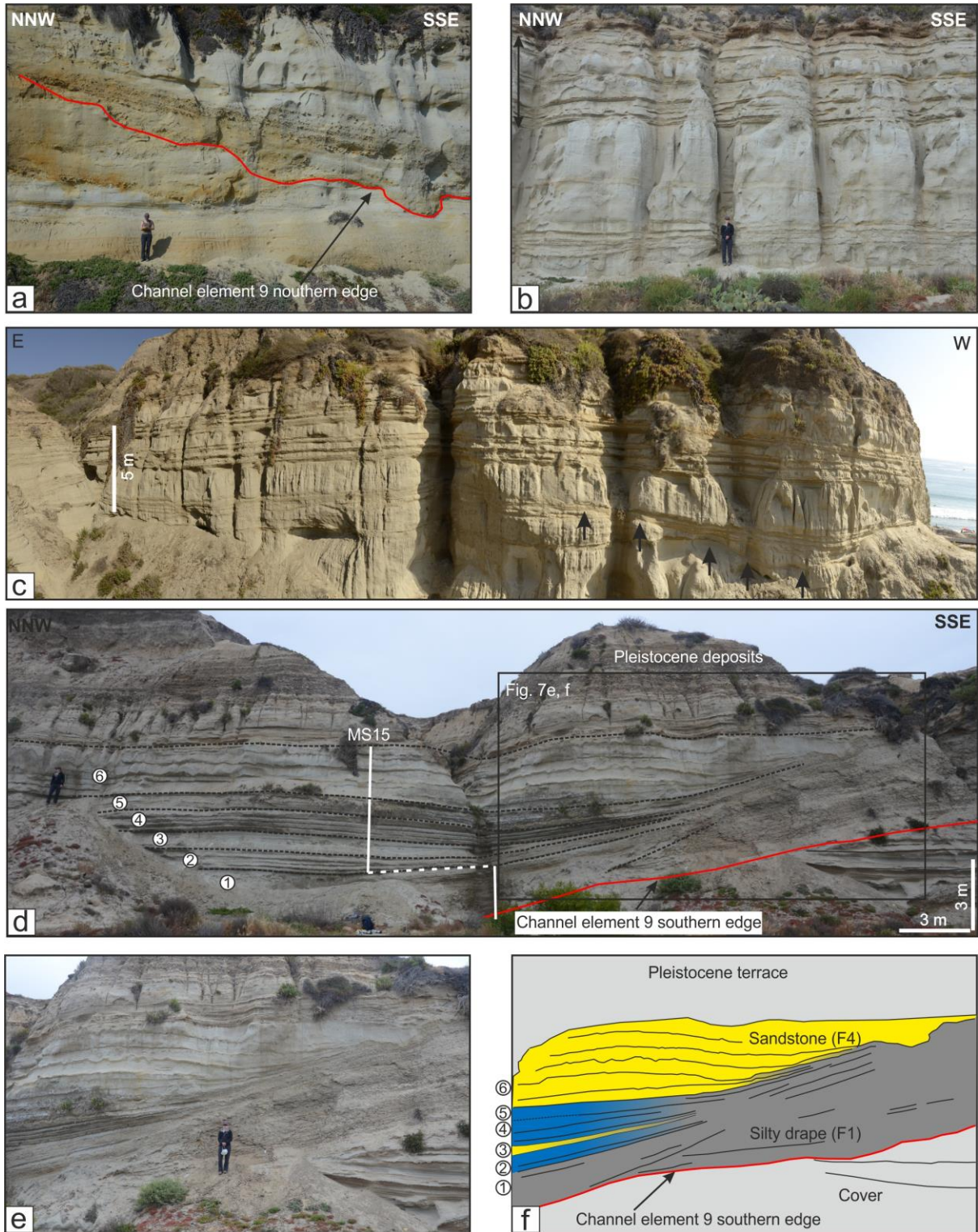


Figure 7

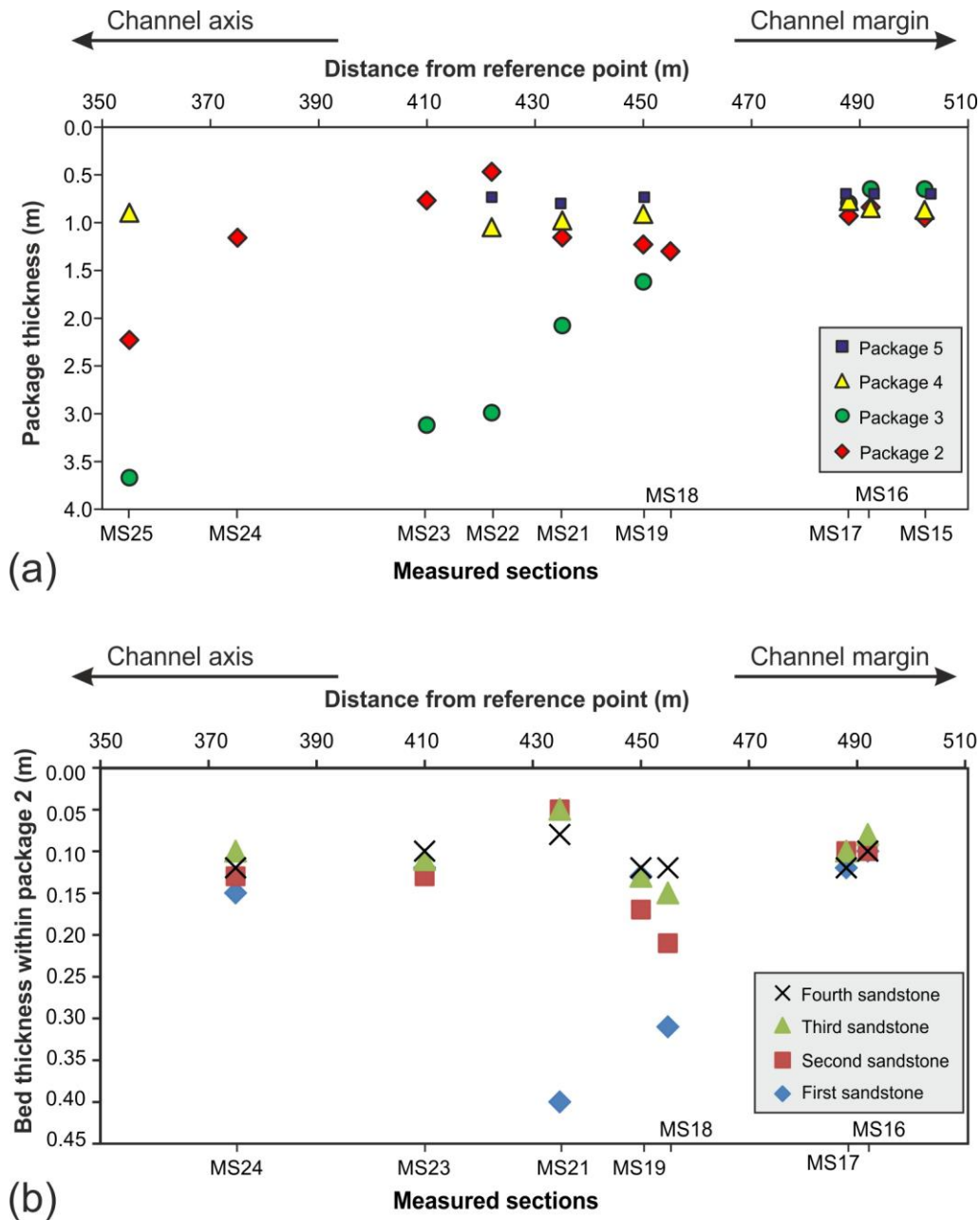


Figure 8



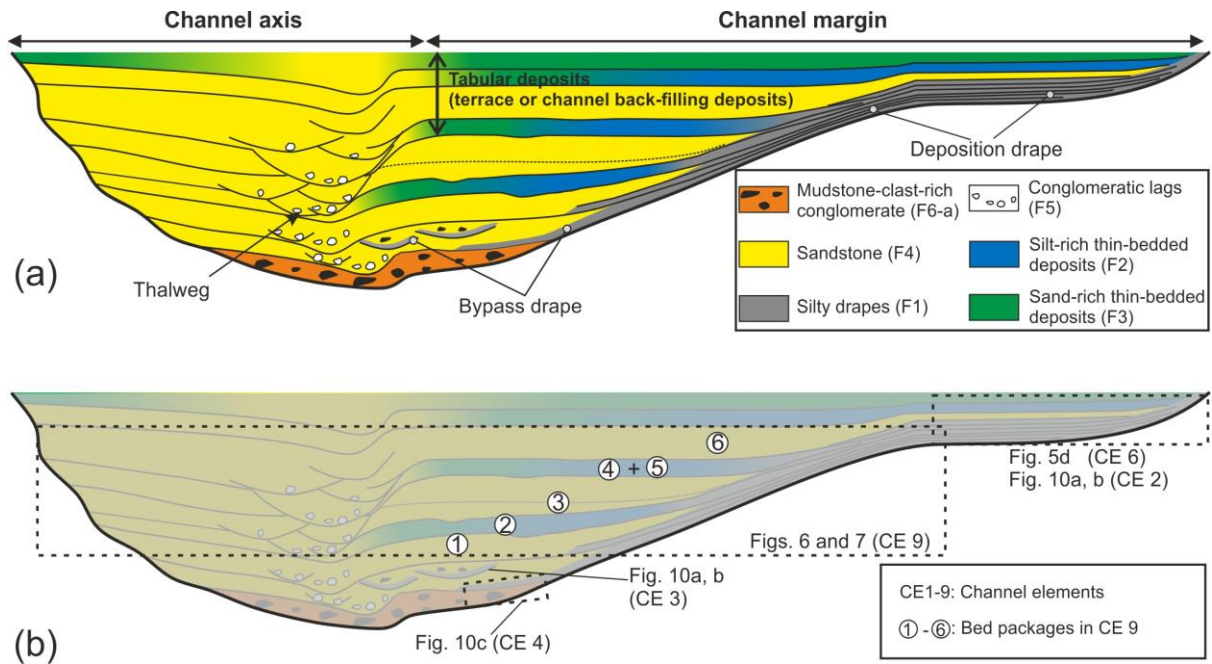


Figure 9

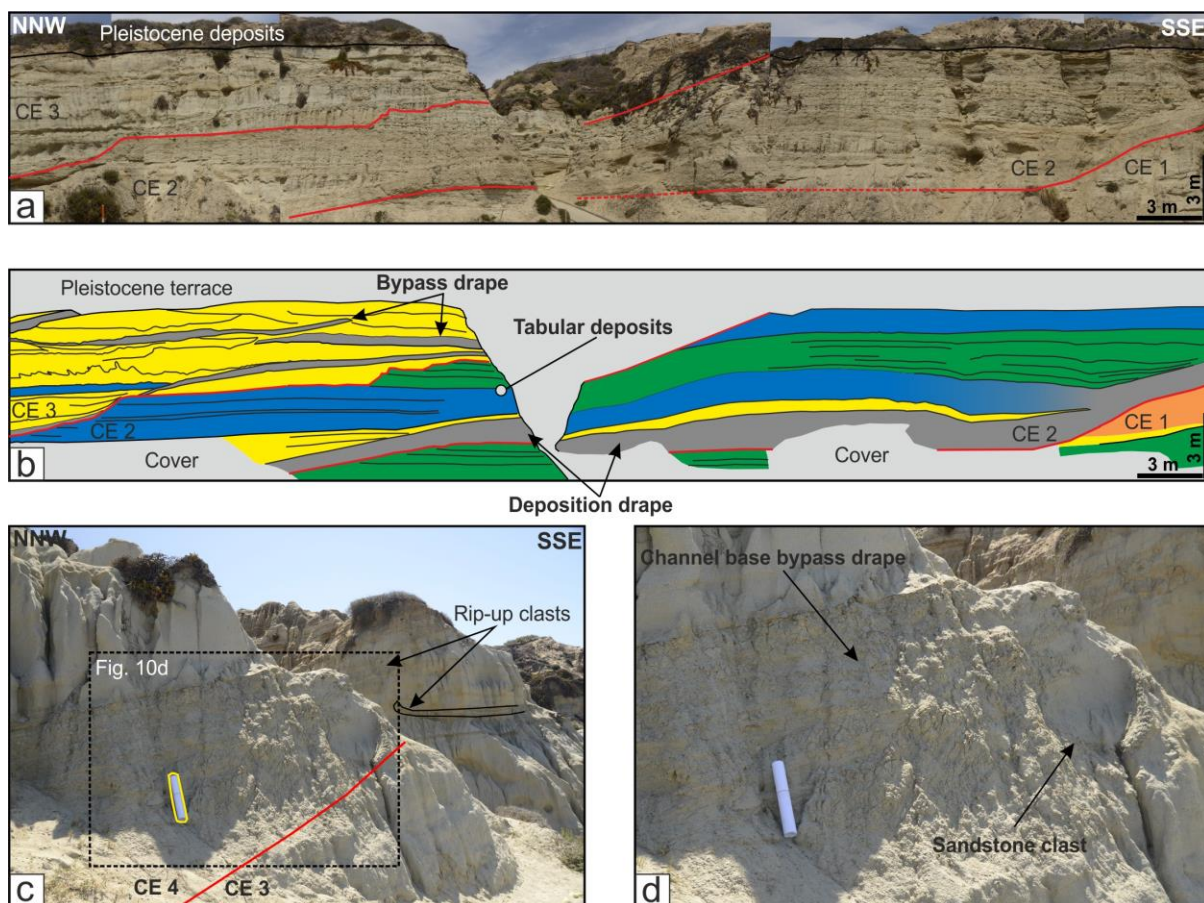


Figure 10

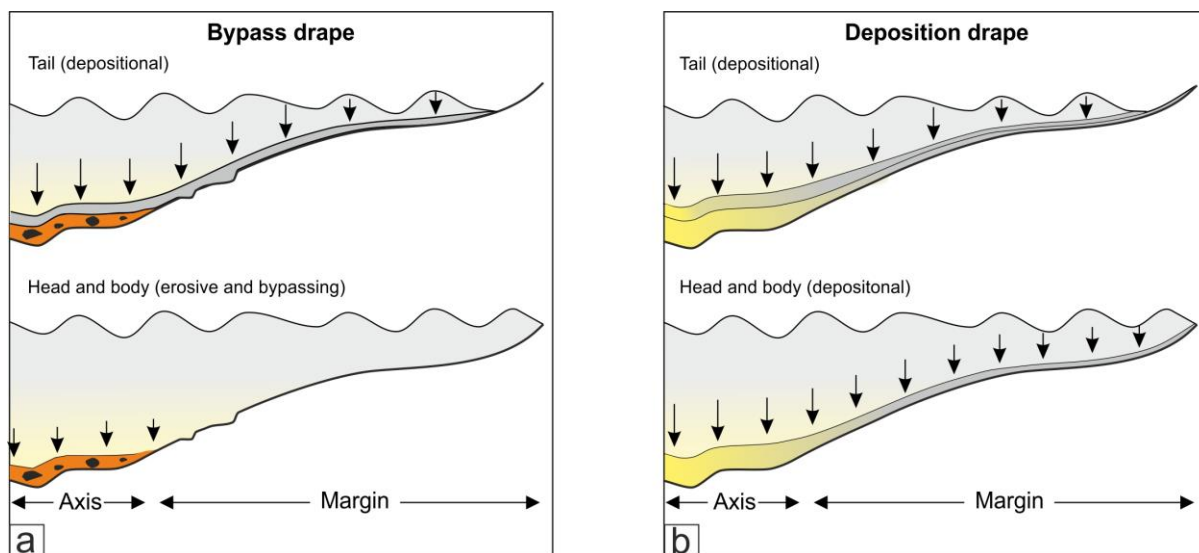
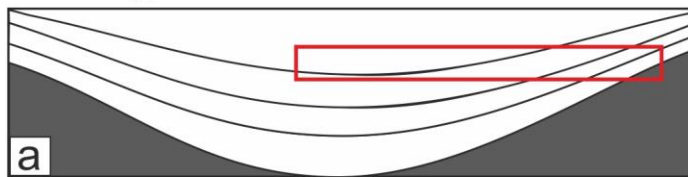


Figure 11

## Vertical aggradation



## Lateral migration

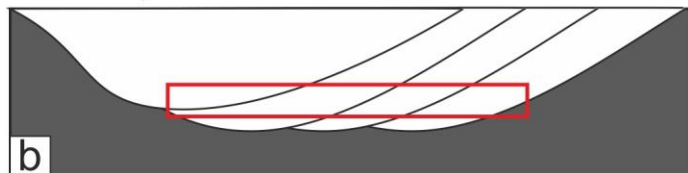


Figure 12

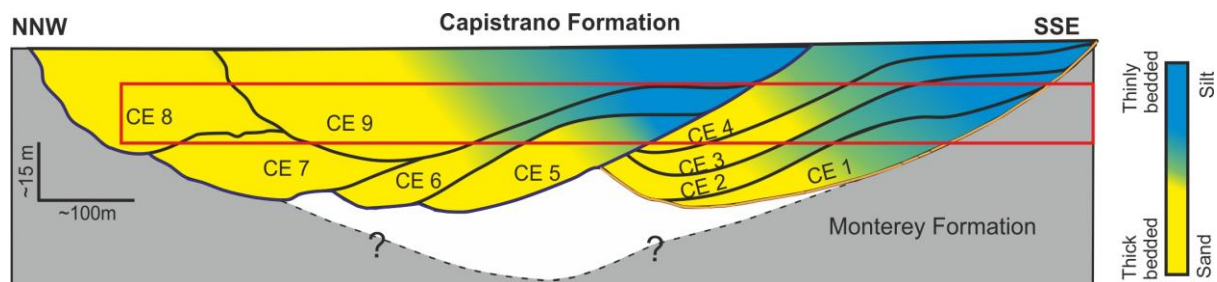


Figure 13



Table 1

<b>Facies</b>	<b>Characteristic grain size</b>	<b>Grading &amp; sedimentary structures</b>	<b>Secondary features</b>	<b>Bedding patterns</b>	<b>Depositional processes</b>
<b>F1</b> Bedded siltstone	Clay and silt (>80%), very fine- to fine- grained sand (<20%)	Commonly normally graded, parallel laminated or massive when strongly bioturbated	Moderate to strong bioturbation	Thinly bedded (1-5 cm) mud-silt or silt-very fine-grained sand couplets with no amalgamation, stacking up to 2.5 m thick units, draping channel or low-relief, intra-channel erosional surfaces	Slow deposition from waning, low - concentration turbidity currents
<b>F2</b> Silt-rich thin-bedded deposits	Clay to medium-grained sand, sand generally makes up 20% to 60%	Commonly normally graded, Parallel or ripple laminated or massive when strongly bioturbated	Minor to strong bioturbation, low diversity, low abundance trace fossil assemblages, commonly injected by adjacent medium- bedded sandstone	Thinly interbedded (<10 cm) mudstone and sandstone with no or rare amalgamation, stacking up to 2 m thick, readily mappable units up to 100-120 m long	Slow deposition from non-erosive, waning, low-concentration turbidity currents
<b>F3</b> Sand-rich thin-bedded deposits	Clay to very coarse- grained sand; sand makes up 60-80%	Largely normally graded Sand: massive, laminated, or transition upward from massive to laminated; Silt: parallel laminated or apparently massive when strongly bioturbated	Minor to moderate bioturbation, soft-deformation structures (slumps, loading structures, convolution bedding)	Thinly bedded (5-20 cm) mudstone and sandstone with a low frequency of amalgamation, stacking up to 3-5 m units, often transitioning into silt-rich thin- bedded deposits and non-to semi amalgamated sandstone laterally.	Slow-to-relatively quick deposition from non-erosive, waning, low-to high-concentration turbidity currents
<b>F4</b> Medium- to thick-bedded sandstone	Dominantly fine to very coarse-grained sand (>80%), with or without conglomerate (<5%) and/or mudstone (<15%)	Coarse-tail grading or ungraded, predominantly massive with or without thin, laminated tops, locally preserved dune-scale cross bedding	Moderately sorted, biotite rich, common presence of mudstone-clasts, soft sediment deformation structures (sand injections, loading structures, and water escape structures)	Medium-to thick - bedded (30 cm-1.2 m), highly amalgamated or non-to semi-amalgamated, stacking up to 5-9 m thick units.	Quick deposition from non-erosive/ erosive, quasi-steady or waning low- to high-concentration turbidity currents
<b>F5</b> Thin- to thick-bedded conglomerate	Primarily pebble to cobble-sized extraformational conglomerates	Ungraded or normally graded Crudely stratified/bedded or massive	Poorly to moderately sorted, subrounded to rounded clasts, poorly to moderately sorted matrix comprising very fine-to very coarse-grained sand, clast/matrix-supported	Thin- to thick-bedded, typically characterized by erosive bases, abundant internal scours, rip-up mudstone clasts and lenticular bed geometries, tending to underlie medium-to thick-bedded sandstone	Deposition from erosive, bypassing, gravely, high-concentration turbidity currents
<b>F6</b> Mudstone-	Granule-to boulder- sized	Largely ungraded Mudstone-clast-rich	F6-a: sub-angular to angular clasts,	F6-a: overlain by conglomerate of F5	F6-a: localized channel margin

---

clast-rich conglomerate (F6-a); mudstone-clast-rich sandstone (F6-b)	mudstone clasts, very fine to coarse grained sand or pebbly sand matrix	conglomerate (F6-a): massive Mudstone-clast-rich sand (F6-b): locally crudely stratified	poorly sorted, matrix-supported F6-b: sub-angular to sub-rounded clasts, moderately sorted, matrix-supported	F6-b: interbedded with medium-to coarse-grained massive sandstone and/or laminated sandstone	slump or freezing of clast-laden turbidity current; F6-b: bypassing turbidity currents
--	---	---	---	--	---



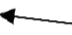






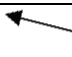

---

ACCEPTED MANUSCRIPT

Table 2

		<b>Bypass drapes</b>	<b>Deposition drapes</b>
<b>Recognition criteria</b>	<b>Grain size</b>	Silt to medium-grained sand	Silt to very fine-grained sand
	<b>Erosion/bypass features</b>	Common e.g., mudstone rip-up clasts, multiple erosional surfaces including channel bases, coarse- grained facies	Non to rare Underlying channel bases are often the only erosional features associated with depositional drapes
	<b>Bed dips</b>	No systematic upward changes	Commonly shallow up
	<b>Lateral facies relationship</b>	Do not grade laterally into axial sandstones	Grade laterally into axial sandstone
	<b>Distribution</b>	Channel margin and/or channel axis	Channel margin
<b>Origins</b>	<b>Formative mechanisms</b>	Tails of bypassing turbidity currents	Upper dilute portions of depositional turbidity currents
<b>Prediction</b>	<b>Time equivalent sands</b>	Mainly downdip	Mainly towards the channel axis

Table 3

Channel element	Channel edge orientation		Paleoflow direction	
	Mean	Data	Mean	Data
1	310° 	310°	324°	 n=7
2	277° 	270°, 284°	312°	 n=4
3	274° 	268°, 280°		
4	290° 			
5	237.5° 	235°, 240°		
6	252° 	240°, 264°		
7				
8			231°	 n=6
9	284° 	275°, 288°, 290°	318.5°	 n=11

## Highlights

- Submarine channel-fills with facies architectural asymmetry and varying stacking patterns are documented.
- Two end-member types of drapes (bypass drapes vs. deposition drapes) are present in the channel fills.
- Bypass drapes and depositional drapes are characterized by different character, genesis and recognition criteria.
- This study presents new insights into submarine channel facies architecture which are applicable to hydrocarbon reservoirs.